

Interplay of interchain interactions and exchange anisotropy: Stability and fragility of multipolar states in spin- $\frac{1}{2}$ quasi-one-dimensional frustrated helimagnets

Satoshi Nishimoto,^{1,2} Stefan-Ludwig Drechsler,^{1,*} Roman Kuzian,^{1,3,4} Johannes Richter,⁵ and Jeroen van den Brink^{1,2}

¹*Institute for Theoretical Solid State Physics, IFW Dresden, Helmholtzstrasse 20, D-01069 Dresden, Germany*

²*Department of Physics, TU Dresden, D-01062 Dresden, Germany*

³*Institute for Problems of Materials Science NASU, Krzhizhanovskogo 3, 03180 Kiev, Ukraine*

⁴*Donostia International Physics Center (DIPC), ES-20018 Donostia-San Sebastian, Spain*

⁵*Universität Magdeburg, Institut für Theoretische Physik, D-39016 Magdeburg, Germany*

(Received 22 December 2012; revised manuscript received 3 November 2015; published 10 December 2015)

We quantify the stability of the formation of multipolar states against always present interchain couplings in quasi-one-dimensional spin- $\frac{1}{2}$ chain systems with a frustrating in-chain J_1 - J_2 exchange, including parameter regimes that are of direct relevance to many edge-shared cuprate spin-chain compounds. Three representative types of antiferromagnetic interchain coupling and the presence of uniaxial exchange anisotropy are considered. The magnetic phase diagrams are determined by density matrix renormalization group calculations and completed by very accurate analytic and numerical results for the nematic and the dipolar phases employing the hard-core-boson approach. We establish that a sizable interchain coupling has a strong influence on the possible instability of multipolar phases at high magnetic fields in the vicinity of the saturation fields in favor of the usual dipolar one-magnon phase. Moreover, skew interchain couplings strongly affect the pitch of spiral states. Our theoretical results bring to the fore candidate materials close to quantum nematic/triatic ordering.

DOI: [10.1103/PhysRevB.92.214415](https://doi.org/10.1103/PhysRevB.92.214415)

PACS number(s): 75.10.Jm, 75.10.Pq

I. INTRODUCTION

In a system with frustrated magnetic interactions, entirely new ground states (GSs) can emerge from the ensuing competition. The geometric frustration of classical Ising spins on a pyrochlore lattice, for instance, results in the famous spin-ice state, the excitations of which are magnetic monopoles [1]. In frustrated quantum magnets and/or in the vicinity of critical points a rich variety of equally interesting and challenging exotic states such as spin liquids, valence-bond crystals, or nematic phases can occur [2–4]. For example, very recently a nematic-like behavior below a wide $1/3$ magnetization plateau has been observed in volborthite [5,6], which is a frustrated magnetic quasi-two-dimensional (2D) kagome lattice compound. In the context of the present paper this example is instructive and encouraging in the sense that theoretical scenarios developed initially for a pure low-dimensional (2D) model can survive also in the 3D case with a small but significant magnetic coupling between the low-dimensional (planar) subsystems. In quantum spin chain systems, in particular, the competition between short- and longer-range magnetic couplings is a common source of frustration, a canonical example of which is the J_1 - J_2 spin- $\frac{1}{2}$ chain [2,3]. Having antiferromagnetic (AFM) next-nearest-neighbor (NNN) interactions ($J_2 > 0$), it is frustrated irrespective of the sign of the nearest-neighbor (NN) coupling J_1 ; see Fig. 1(a). In the classical J_1 - J_2 spin chain the competing interactions generate a helimagnetic state but in a single chain quantum fluctuations destroy the long-range helical order. For sufficiently high magnetic field, for any value of J_1 , the FM state takes over and the system's magnons, its propagating spin flips, become its exact single-particle excitations. The exchange parameters J_1 and J_2 determine the

magnon dispersion and the *interaction* between them. An AFM NN exchange coupling leads to a repulsion between magnons, whereas a FM NN coupling results in an attraction, which favors the formation of magnon bound states. For a frustration ratio $\alpha = -J_2/J_1 > 0.367$ an interesting and intensely studied nematic state can occur, which may be thought of as a condensate of 2-magnon bound states [7–16] characterized by a quadrupole spin order with a nonzero anomalous average $\langle \hat{S}_i^+ \hat{S}_j^+ \rangle$. For $1/4 < \alpha < 0.367$ also three-, four-, and even higher magnon bound states can condense, resulting in a rich phase diagram with quite a number of exotic magnetic multipolar phases (MPPs).

These theoretical developments have stimulated an experimental quest to find multipolar condensates in quasi-one-dimensional (1D) magnetic materials, in particular, in spin $s = \frac{1}{2}$ systems consisting of edge-shared copper-oxide chains, such as LiVCuO₄ (in cuprate notation \equiv LiCuVO₄ in traditional chemical notation) [14,17–21], Li₂ZrCuO₄ [22,23], Ca₂Y₂Cu₅O₁₀ [24,25], PbCuSO₄(OH)₂ [21,26–28] (linarite), Rb₂Cu₂Mo₃O₁₂ [29], and Li₂CuO₂ [30,31].

Except for the famous spin-Peierls system CuGeO₃ with an enhanced NN AFM superexchange due to an unusually large Cu-O-Cu bond angle and a significant crystal field anisotropy, in these systems J_1 is intrinsically FM and J_2 can be of comparable strength, but it is always AFM. In real 3D materials, however, a magnetic interchain (IC) interaction is unavoidably present. Due to the fragility of purely 1D bound states, IC interactions can readily pose a relevant perturbation to a multipolar state, even when its coupling strength is relatively small [31], i.e., an order of magnitude smaller than the intrachain couplings. To establish the consequences of this key ingredient for the stability of MPPs we consider here the three most common types of IC couplings J^{IC} that are encountered in the quasi-1D edge-shared cuprates mentioned above (one perpendicular IC coupling and two different types of skew

*s.l.drechsler@ifw-dresden.de

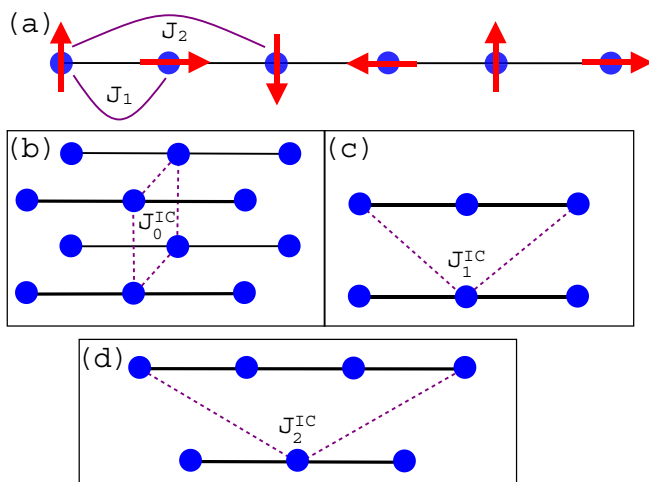


FIG. 1. (Color online) (a) Competing NN and NNN exchange J_1 and J_2 , respectively, along a chain. Coupling between different chains: (b) perpendicular coupling J_0^{IC} , (c) skew (diagonal) coupling J_1^{IC} [e.g., $\text{PbCuSO}_4(\text{OH})_2$], and (d) skew NNN coupling between shifted chains J_2^{IC} (e.g., Li_2CuO_2). The effect of J_0^{IC} is considered in both 2D (e.g., LiVCuO_4) and 3D arrangements.

ones; see Fig. 1) and determine the boundaries of the magnetic phase diagram numerically by density matrix renormalization group (DMRG) calculations and analytically by hard-core boson (HCB) [31–34] and spin-wave (SW) [25] approaches. On top of this we consider also as a first illustrative example the presence of a uniaxial exchange anisotropy focusing on the anisotropy in the NN coupling along the chains, which is believed to be the leading anisotropy term in edge-shared chain cuprates [35–38]. We show that the stability of MPPs is strongly affected by the strength of the AFM IC couplings and depends on the concrete type (geometry) of this coupling, which may also largely affect the pitch of the spiral state. A small easy-axis exchange anisotropy, however, enhances the stability of MPPs dramatically, also in the presence of IC couplings, since it enhances the intrachain attraction between magnons. From the material’s viewpoint based on the presently investigated several members of a still growing family of quasi-1D J_1 - J_2 compounds, our theoretical results bring to the fore linarite, $\text{PbCuSO}_4(\text{OH})_2$, as a promising and experimentally convenient [26,28] candidate compound with a triatic MPP, which can be stabilized by its sizable exchange anisotropy, and confirm the closeness of LiVCuO_4 to quantum nematicity. It is noteworthy that for both compounds the expected neighboring phases of anomalous longitudinal collinear spin density waves SDW_p with $p \geq 2$, where the parameter $p = 2, 3, 4, \dots$ denotes the character of the expected adjacent MP order at higher fields up to saturation, have been detected and analyzed recently [39–42]. These anomalous SDW_p -ordered phases are characterized by a magnetization-dependent propagation wave vector [cosine-like (sine-like) spin modulated phases] with zero transverse magnetization. It is also noteworthy that the expected nematicity-related adjacent case $p = 2$ has been observed for LiVCuO_4 [42] whereas multiple SDW_p phases in different field and temperature regions in the complex phase diagram have been reported for

linarite [39]. But the existence of their corresponding expected counterparts, namely the nematic states at higher fields, has very probably not yet been settled experimentally, even in the simpler nematic case of LiVCuO_4 [40,41], in contrast to the assigned there detection of a bond-nematic phase by Mourigal *et al.* [42]. For completeness we mention that the possibility of coexisting nematic and SDW_2 phases after a second-order phase transition at slightly lower fields has been suggested in Ref. [43] using the approximate dilute Bose gas approximation based ladder summation also at *finite* pair densities, but this case of a homogeneous coexistence of both competing phases was explicitly excluded in Refs. [40,41] based on rather general field-theory-based arguments.

Our paper is organized as follows. In Sec. II we specify the models considered here and briefly illustrate the methods used to analyze them. In Sec. III we present our main theoretical results. The relation of our theoretical findings to concrete edge-shared cuprate spin-chain compounds is discussed in Sec. IV. In particular, based on our theoretical analysis we propose possible candidate compounds to find experimentally more MPPs and discuss in this context how to influence the MPPs by external stress or pressure. We summarize our findings in Sec. V. In order to focus on the obtained results and their discussion in the main text, we provide technical details of our hard-core boson (HCB) approach in Appendices A and B.

II. MODELS AND METHODS

The general relevant Hamiltonian

$$H = H_{1D} + H_{IC} \quad (1)$$

considered here encompasses in the simplest form the frustrating magnetic interactions along the 1D chain in the presence of an external magnetic field h and a small uniaxial NN exchange anisotropy $\Delta_1 \neq 1$,

$$H_{1D} = \sum_{n,i} [-\mathbf{S}_{n,i} \cdot \mathbf{S}_{n,i+1} + \alpha \mathbf{S}_{n,i} \cdot \mathbf{S}_{n,i+2}] - \sum_{n,i} [(\Delta_1 - 1) S_{n,i}^z S_{n,i+1}^z + h S_{n,i}^z], \quad (2)$$

where n labels the chain and i the position of the spins along the chain. Neighboring chains n and m interact via

$$H_{IC} = \sum_{(nm),r} J_r^{IC} \mathbf{S}_{n,i} \cdot \mathbf{S}_{m,i+r}, \quad (3)$$

where $r = 0$ corresponds to a perpendicular IC coupling and $r = 1, 2$ refer to skew IC couplings; see Fig. 1. We use $|J_1|$ as the energy unit for all coupling constants entering our Hamiltonian H . Note that a more general Hamiltonian allowing also uniaxial anisotropies Δ_2 in the NNN and Δ_{IC} in the IC exchange interactions is considered in Appendix A, cf. Eq. (A1), and the effect of these additional anisotropies is also briefly discussed in Sec. III A.

To determine the nature of the magnetic GS and its dependence on the frustration α , the different types of IC exchange J^{IC} , and the exchange anisotropy $\Delta_1 - 1$, we employed the DMRG method [44] with periodic boundary conditions (PBCs) for all directions. This method is not restricted to purely 1D and can also be used for 2D [45,46] and 3D [31,34]

systems, although the system size is limited, e.g., up to about $\sqrt{N} \times \sqrt{N} \times L = \sqrt{10} \times \sqrt{10} \times 50$ for spin Hamiltonians. We kept $p \approx 800$ –5000 density-matrix eigenstates in the renormalization procedure. About 100–300 sweeps are necessary to obtain the GS energy within a convergence of $10^{-7} J_1$ for each p value. All calculated quantities were extrapolated to $p \rightarrow \infty$ and the maximum error in the GS energy is estimated as $\Delta E/J_1 \sim 10^{-4}$, while the discarded weight is less than 1×10^{-6} . Under the PBCs, a uniform distribution of $\langle S_i^z \rangle$ may give an indication to examine the accuracy of DMRG calculations for spin systems. Typically, $\langle S^z \rangle - S_{\text{tot}}^z/(NL)$ is less than 1×10^{-3} in our calculations. Note that for high-spin states [$S_{\text{tot}}^z \gtrsim (NL - 10)/2$] the GS energy can be obtained with an accuracy of $\Delta E/J_1 < 10^{-12}$ by carrying out several thousand sweeps even with $p \approx 100$ –800. We considered systems with different lengths: $L = 16$ –64 (24–96) for 3D (2D) and adopted power laws to perform a finite-size-scaling analysis. From this we obtained the saturation field h_s in the thermodynamic limit $L \rightarrow \infty$. As a result, we obtain h_s with high accuracy.

In addition to DMRG we have also applied an analytic HCB approach [32] to provide exact results for the nematic and dipolar phases. This approach is based on the simple observation that magnons are the single-particle excitations above the fully polarized FM state at high magnetic fields. The problem of an interacting pair of particles is reduced to a one-particle problem of the motion in an effective potential well. In our case it corresponds to an impurity problem in a tight-binding Hamiltonian explained in more detail in Appendix A, including Fig. 13. In addition, some of the calculated magnetization curves have been cross-checked by exact diagonalizations possible for corresponding finite systems with periodic boundary conditions.

III. RESULTS

A. Perpendicular interchain coupling between unshifted chains

The simplest case, relevant for, e.g., LiVCuO₄ and Li(Na)Cu₂O₂, is the situation of unshifted neighboring chains and a perpendicular interchain exchange J_0^{IC} ; see Fig. 1(b). In this case spirals on NN chains are only weakly affected by an AFM IC coupling [47]; on a classical level the pitch of the incommensurate (INC) spiral state is not affected by J_0^{IC} . This is in stark contrast to the effect of skew AFM J_1^{IC} and J_2^{IC} , which can strongly reduce the pitch.

A typical magnetization curve for $\alpha = 0.5$ and $\Delta_1 = 1$, for a nematic phase, is shown in Fig. 2. The height of the magnetization steps $\Delta S^z = 2$ when $J_0^{\text{IC}}/\alpha = 0.1$ is the direct signature for 2-magnon bound states. At larger values of the IC coupling these bound states are suppressed, as is clear from the magnetization curve for $J_0^{\text{IC}}/\alpha = 0.2$, where the steps correspond to $\Delta S^z = 1$. So in the isotropic case, where $\Delta_1 = 1$, a rather weak critical IC coupling as compared to $|J_1|$ destroys the nematic phase in favor of the usual conical ordering. Within the picture of ferromagnetically coupled interpenetrating simple AFM Heisenberg chains, it is convenient to measure the IC in terms of J_2 ; i.e., as J_0^{IC}/α and to use $1/\alpha$ instead of α as has been done in Figs. 2, 4, and 9. At $\alpha = 0.5$ the critical value for J_0^{IC}/α amounts 0.188 (0.088) in 2D (3D), respectively. This value of α is near the maximum of J_0^{IC}/α (see

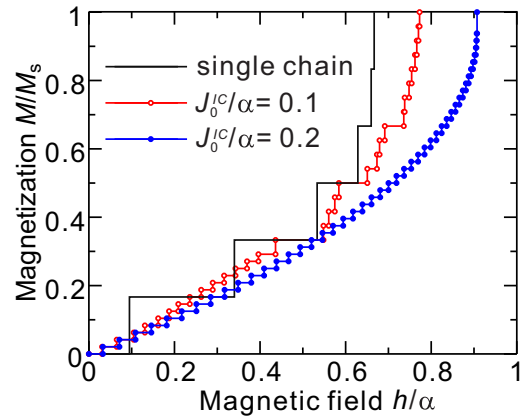


FIG. 2. (Color online) Magnetization vs magnetic field for a 2D arrangement of four chains with $N = 24$ sites each, with a perpendicular IC coupling J_0^{IC} [cf. Fig. 1(b)], $\alpha = 1/2$, and $\Delta_1 = 1$ (isotropic case).

Figs. 4 and 9). Notice a formal shift of the maximum position to more than twice as large α values, if J_0^{IC} is traditionally measured in units of $|J_1|$ and plotted as a function of the inverse value α (see Fig. 10). Thereby also its shape and height are changed: for example from 0.088 to 0.07056 in the 3D case.

The consideration of the excitation spectra at fields at or exceeding the saturation field gives another point of view on the MPPs. The spectral density of the two-particle Green's function is depicted in Fig. 3 for the 2D case. The sharp peaks below the two-particle continuum correspond to bound pairs of magnons. The bound-state energy and the continuum boundaries depend on the total momentum of a pair \mathbf{k} . If the bound-state energy minimum lies below the lowest continuum energy, the bound pairs may condense at magnetic fields just below the saturation field. The condensate of pairs forms the nematic state of the magnetic system [7,15]. We see that for small IC couplings J_0^{IC} the spectral density behaves qualitatively similarly to the 1D case (upper panel of Fig. 3); i.e., the peak corresponding to a bound pair lies below the continuum, and its dispersion exhibits a minimum at the total momentum $\mathbf{k}\mathbf{a} = \pi$ of a pair (middle panel of Fig. 3). In the lower panel of Fig. 3 we see that the behavior of the spectral density changes for large enough IC. The bound state is still present near the edge of the Brillouin zone, but its energy is higher than the minimum of the two-particle continuum. In this case, *single* magnons will condense at magnetic fields below the saturation field, and form the dipolar phase.

The full phase diagram [48] is shown in Fig. 4, where the phase boundaries are extracted from the kinks in the calculated saturation field h_s as a function of J_0^{IC} , as shown in Figs. 4(a)–4(c). Clearly, the three-, four-, and higher magnon MPPs are even more strongly affected by the IC interaction.

Except for the obvious strong influence of the IC coupling J_0^{IC} there is also a substantial effect of a finite uniaxial exchange anisotropy, $\Delta_1 - 1 \neq 0$, on the stability of the MPP [see the symbols in Fig. 4(d) at $(1/\alpha) = 2$]. Note that the anisotropy in the NN exchange $\Delta_1 - 1$ is the leading-order anisotropy in the cuprate spin-chain compounds (according to theoretical microscopic studies for quasi-1D cuprates [35,36]). Figure 4(d) shows that for $\alpha = 0.5$ a moderate anisotropy

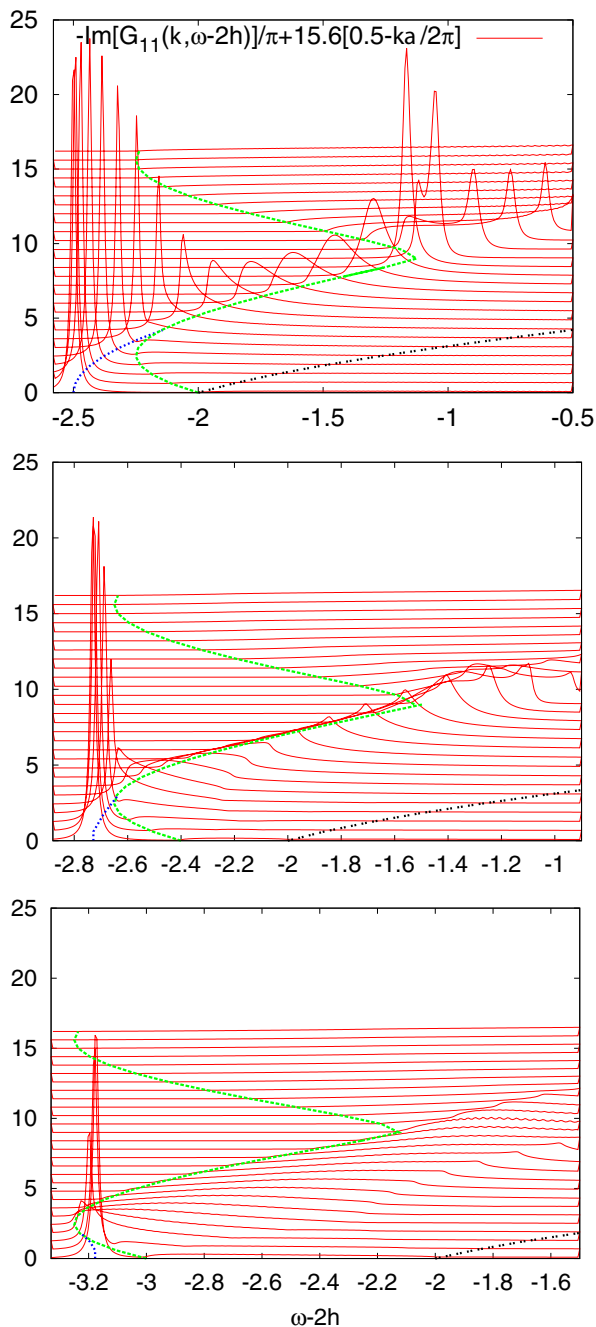


FIG. 3. (Color online) The spectral density of the two-particle Green's function as a function of the wave vector \mathbf{k} (parallel to the chain direction **a**) and of the energy ω for a 2D arrangement of unshifted J_1 - J_2 chains, a perpendicular IC interaction J_0^{IC} (upper, middle, and lower panels correspond to $J_0^{\text{IC}} = 0, 0.1$, and 0.25 , respectively) and $\alpha = 1$ ($J_2 = -J_1$). The spectral density graphs are shifted vertically, where the shift is proportional to $\pi - \mathbf{k}\mathbf{a}$. On each panel, the lowest (highest) graph corresponds to $\mathbf{k}\mathbf{a} = \pi$ ($\mathbf{k}\mathbf{a} = -\pi/26$). A small imaginary part $\eta = 0.01$ was added to ω in order to visualize the δ -function peaks corresponding to bound states. The green dashed (black double dotted) line shows the lower (upper) boundary of the 2-magnon continuum. The blue dotted line shows the 2-magnon bound state dispersion $\omega_b(\mathbf{k}\mathbf{a})$. The line in the upper panel is given by an analytic expression (see Eqs. (38) and (39) in Ref. [32]) $\omega_b(\mathbf{k}\mathbf{a}) = \omega_b(\pi) + (\mathbf{k}\mathbf{a} - \pi)^2/2m_{\text{eff}}$. In the other panels the lines showing $\omega_b(\mathbf{k}\mathbf{a})$ have been found numerically.

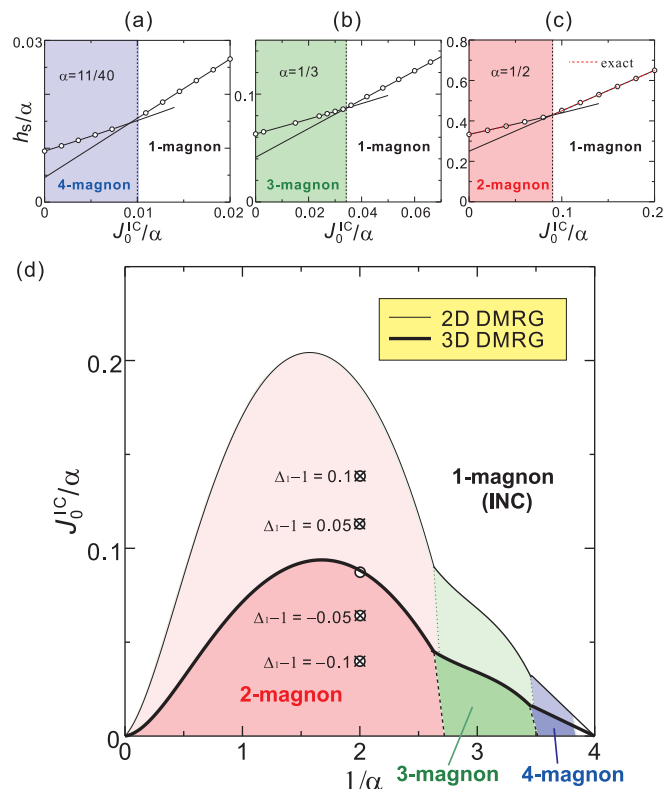


FIG. 4. (Color online) DMRG-derived phase diagram for unshifted chains with perpendicular IC coupling. (a)–(c) Saturation field h_s as a function of the perpendicular IC coupling J_0^{IC} [cf. Fig. 1(b)] and $\Delta_1 = 1$. (d) Phase diagram with critical IC coupling in 3D (thick line) and 2D (thin line). The phase boundaries are extracted from the kinks in the saturation field h_s ; cf. panels (a)–(c). Symbols: The dependence of the critical J_0^{IC} on the uniaxial exchange anisotropy $\Delta_1 - 1 > 0$ in 3D for $\alpha = 0.5$, where \circ/\times correspond to the DMRG/HCB results, respectively.

of $\Delta_1 - 1 = 0.1$, only, increases the critical IC coupling by a factor of ~ 1.6 , and thus significantly enhances the MPP stability region.

Now we will discuss in more detail some approximate analytical results obtained within the framework of our HCB approach which provides, in contrast with the standard situation in many-body physics with a complex ground state, a restricted finite set of (closed) equations expanded analytically by treating the interchain interaction in various orders of the perturbation theory. The derivation of the phase boundary between the one- and two-magnon instabilities relies first of all on the derivation of the saturation fields for these two instabilities, $h_{s,1}$ and $h_{s,2}$, respectively. Requiring

$$h_{s,2} = h_{s,1} \quad (4)$$

then renders the equation for the critical IC J_{cr} coupling as a function of the anisotropy and the frustration parameters. The saturation field $h_{s,1}$ of the INC phase on the one-magnon side is described already within the SW theory (see Appendix B):

$$h_{s,1} \equiv -\Delta_1 + (1 + \Delta_2)\alpha + \frac{1}{8\alpha} + \frac{N_{\text{IC}}}{2}(J_0^{\text{IC}}\Delta_{\text{IC}} + |J_0^{\text{IC}}|), \quad (5)$$

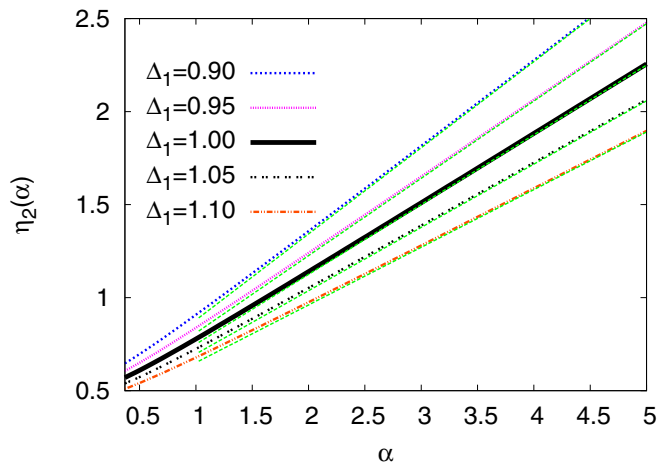


FIG. 5. (Color online) The second-order expansion coefficient η_2 as a function of the frustration parameter α and various exchange anisotropies Δ_1 . The green dashed lines show the large α asymptotics $3(1 + \alpha/\Delta_1)/8\Delta_1$.

where N_{IC} denotes the number of IC neighbors (i.e., for J_0^{IC} in 3D and 2D, $N_{IC} = 4$ and 2 , respectively). We note that, in principle, $N_{IC} = 3, 4$, and 6 are relevant for alternative 3D-chain arrangements, i.e., for hexagonal, kagome, and triangular chain lattices, respectively. However, to the best of our knowledge for the type of the frustrated edge-shared cuprate chain compounds under consideration such chain structures have not been found hitherto, although several triangular (but unfrustrated or both NN and NNN ferromagnetic couplings along the chain directions) examples are known. Hence, these so far academically interesting cases with possible additional frustrations perpendicular to the chains for antiferromagnetic interchain couplings will not be considered here.

From Eq. (5) it is obvious that for an isotropic FM IC coupling, i.e., for $J_0^{IC} < 0$ and $\Delta_{IC} = 1$, the saturation field $h_{s,1}$ does not depend on J_0^{IC} at all; cf. Ref. [32].

For the nematic phase we are able to obtain *exact* values for $h_{s,2}$ using the HCB approach [32]. The HCB values are in accord with the DMRG results (see Figs. 5 and 10). In the limit $J_0^{IC} \ll 1$ we arrive at a fastly converging expansion with relatively simple analytical expressions for the leading coefficients

$$h_{s,2} = h_{s,2}^{1D} + \frac{N_{IC}}{2} J_0^{IC} \Delta_{IC} + N_{IC} [\eta_2 (J_0^{IC})^2 + \eta_4 (J_0^{IC})^4 + O(J_0^{IC})^6], \quad (6)$$

where the saturation field of the single chain including both in-chain exchange anisotropies Δ_i , $i = 1, 2$, is given by [32,49]

$$h_{s,2}^{1D} = -\Delta_1 + (1 + \Delta_2)\alpha + \frac{\Delta_1^2}{2(\Delta_1 + \alpha)}. \quad (7)$$

The expansion coefficient η_2 in second order of the IC coupling reads

$$\begin{aligned} \eta_2(\alpha, \Delta_1) &= \frac{(\Delta_1 + \alpha)(3\alpha^2 + 3\alpha\Delta_1 + \Delta_1^2)}{2\Delta_1^2(\Delta_1 + 2\alpha)^2}, \\ &= \frac{3(1 + \frac{\alpha}{\Delta_1})}{8\Delta_1} \left[1 + \frac{1}{3(1 + \frac{2\alpha}{\Delta_1})^2} \right]. \end{aligned} \quad (8)$$

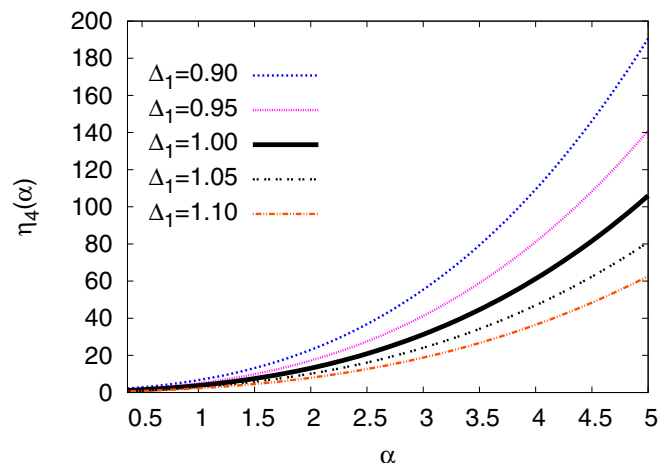
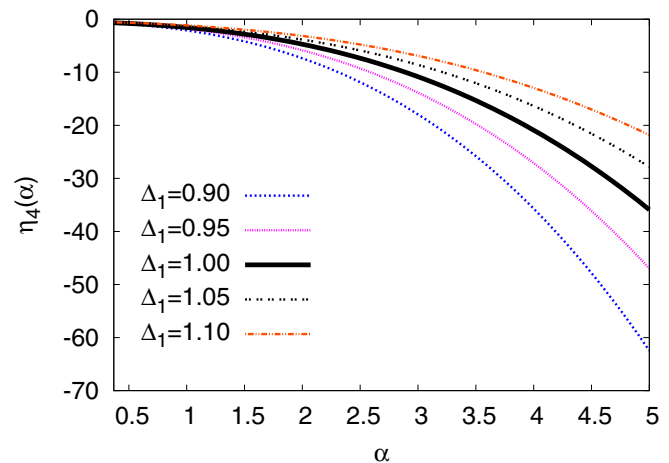


FIG. 6. (Color online) The fourth-order expansion coefficient η_4 as a function of the frustration parameter α and various exchange anisotropies Δ_1 for 2D (upper panel) and 3D (lower panel) systems.

The inspection of the second term within the large parentheses in Eq. (8) and the plot of η_2 in Fig. 5 shows that for $\alpha \gtrsim 0.75$ the η_2 values exhibit a quasilinear behavior governed by the prefactor $3(1 + \alpha/\Delta_1)/8\Delta_1$ in the second equality of Eq. (8). The general derivation of the next relevant coefficient η_4 determining the fourth-order term is provided in Appendix B. The inspection of Eq. (8) shows also that η_2 does not depend on the dimensionality. That is, in the second order, the contributions of neighboring chains sum up independently. Notice that this is not the case for higher orders. In particular, the coefficient η_4 occurs differently for 2D and 3D geometries as shown in Fig. 6.

We show, as an example, in Fig. 7 the saturation field as a function of the IC coupling J_0^{IC} for the 2D case at $\alpha = 1$, i.e., the optimal parameter value for the existence of the nematic phase, where $J_{0,cr}^{IC} \approx 0.1655$. For small J_0^{IC} the second-order expansion reproduces well the DMRG data which coincide with the results from a numerical solution of Eq. (B3). Naturally, for larger interchain coupling $J_0^{IC} > 0.15$ a fourth-order expansion is needed. As a second example we consider a 3D system with uniaxial anisotropy. The dependence of the saturation field on the IC and anisotropy strength is shown in Fig. 8. We see that although Eq. (6) for

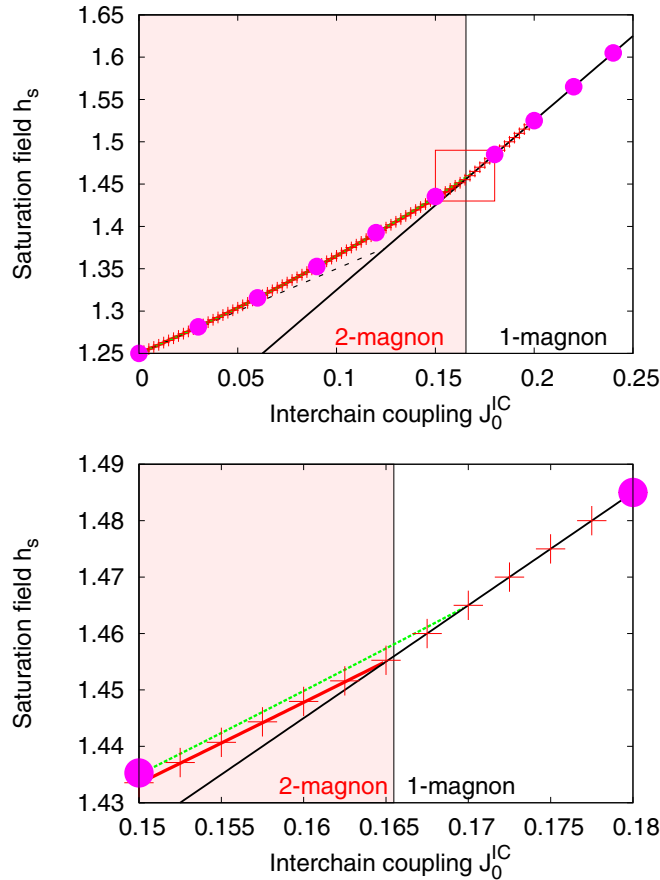


FIG. 7. (Color online) The saturation field h_s for a 2D array of chains for $\alpha = 1$, $\Delta_1 = 1$ (isotropic case) vs IC coupling J_0^{IC} . The notations on both panels: magenta circles, DMRG data; red crosses, HCB data from the numerical solution of the general HCB equations Eq. (B3); black short-dashed, green long-dashed, and thick red solid lines show linear, quadratic, and quartic approximations to $h_{s,2}$ given by Eq. (6), respectively; thin black solid line, the 1-magnon value of $h_{s,1}$ [see Eq. (5)]. The intersections of the $h_{s,2}$ and the $h_{s,1}$ curves yield the values of the critical IC coupling $J_{0,\text{cr}}^{\text{IC}}$. Lower panel: The region around $J_{0,\text{cr}}^{\text{IC}}$, which is denoted on the upper panel by a red rectangle.

$h_{s,2}$ is approximate, it is accurate enough for many practical purposes (see Figs. 4, 8, and 9).

Comparing the expressions for $h_{s,1}$ and $h_{s,2}$ one notices, besides the presence of already mentioned various nonlinear IC terms for the nematic side, that also its linear term differs from that in the usual one-magnon phase. The approximate solution of Eq. (4) with $h_{s,2}$ given by Eq. (6) provides very precise *analytical* expressions for the critical IC interaction $J_{0,\text{cr}}^{\text{IC}}$ above which the nematic phase does not exist. It is noteworthy that for an external magnetic field parallel to the easy axis considered here both anisotropies Δ_2 and Δ_{IC} of the NNN exchange and the IC coupling [see Eq. (6)], as well as the simple linear term in J_0^{IC} in general, drop out and one is left with a polynomial equation in terms of $|J_0^{\text{IC}}|$, only, since there are no higher order odd terms. [Note that the vanishing of the cubic term in J_0^{IC} is shown explicitly in Appendix B; see Eqs. (B29) and (B30).] Then the critical IC coupling coincides for both signs. This somewhat unexpected finding is in accord with the results reported for the 3D case by Ueda and Totsuka in

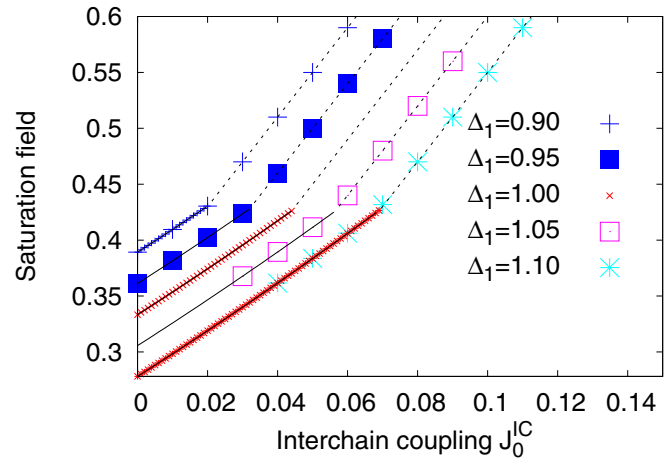


FIG. 8. (Color online) The saturation field h_s for perpendicular IC coupling J_0^{IC} (3D case, i.e., a square-lattice arrangement of unshifted chains), $\alpha = 0.5$, and various values of the easy-plane anisotropy ($\Delta_1 < 1$), as well as easy-axis anisotropy ($\Delta_1 > 1$). Large symbols show DMRG data ($\Delta_1 \neq 1$); small red crosses show the data from a numerical solution of the HCB equation (B3). Solid [dashed] lines show the analytic expression for $h_{s,2}$, Eq. (6) [$h_{s,1}$, Eq. (5)].

Ref. [50] (see Fig. 6 therein) based on a summation of ladder diagrams. We stress that according to our DMRG calculations this remarkable sign independence of the critical IC coupling is valid (i) for very special types of IC geometries such as the NN-perpendicular coupling J_0^{IC} considered here, only, and (ii) for not too strong FM J_0^{IC} values. For stronger negative (i.e., FM) IC couplings above a critical coupling some higher order multimagnon states may become more favorable than the nematic and the one-magnon phase as well. Anyhow, a systematic study of this “strong coupling” FM IC case, to the best of our knowledge not observed in edge-shared chain cuprates, is beyond the scope of the present work.

We can also get physical insight into the role of the IC coupling by the inspection of the effective Hamiltonian derived within the HCB approach and given in Appendix A. Obviously, the IC coupling leads to a D -dimensional ($D > 1$) periodic part of the effective Hamiltonian [see Eq. (A13) in Appendix A]. The enhanced kinetic energy causes a more shallow impurity level (i.e., it diminishes the binding energy of the bound pair). As shown in Appendix B, the effective particle (i.e., internal pair) motion is not affected by the effective impurities corresponding to the IC, while the minimum of the bound-state dispersion occurs at $\mathbf{k}\mathbf{a} = \pi$. This is the reason why the critical value of the IC coupling is *independent* of its sign, while the minimum of the spectrum corresponds to two-particle bound states. In the same context it becomes clear why in general a 2D arrangement is more stable against IC than a 3D one, as mentioned above for the particular case $\alpha = 0.5$. In the FM IC regime the increase of the attractive FM interactions beyond a critical threshold stabilizes a complex higher order multimagnon bound state. Anyhow, since in the majority of the edge-shared chain compounds AFM IC coupling is expected, we will below focus on this case, i.e., $J_r^{\text{IC}} \geq 0$.

After this more general qualitative but rigorous discussion let us now derive simple analytical expressions for the critical

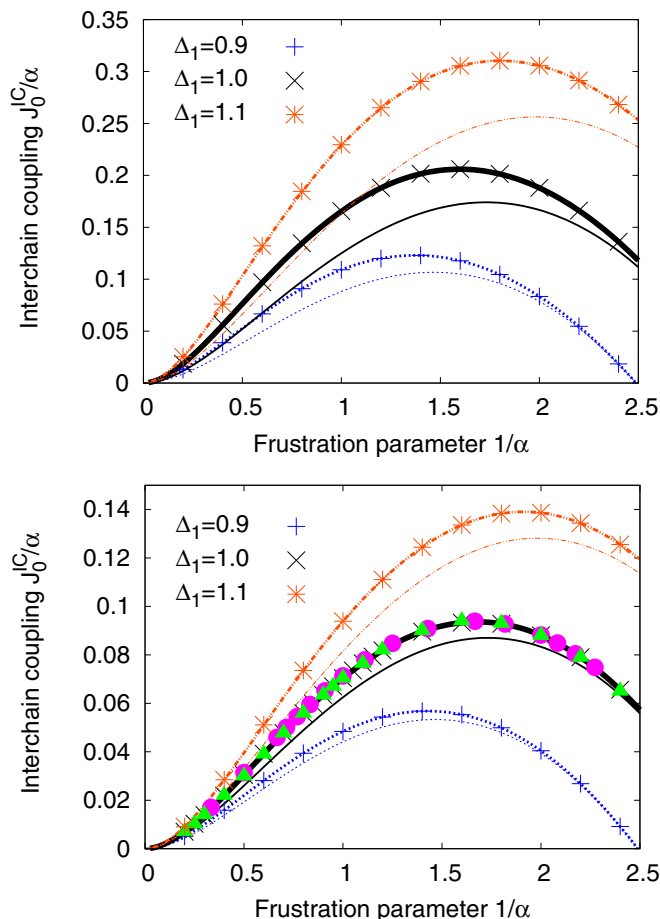


FIG. 9. (Color online) Boundary between the 1- and 2-magnon phases for a system with perpendicular IC coupling J_0^{IC} and various values of the uniaxial anisotropy Δ_1 . Symbols +, \times , and * show the numerical solution of Eq. (B3). Thick curves: $J_{0,cr2}^{\text{IC}}$ from Eqs. (12) and (13); thin curves: $J_{0,cr1}^{\text{IC}}$ from Eq. (9). Upper panel: The 2D case. Lower panel: The 3D case. Green triangles show the results from the summation of ladder diagrams (Ref. [50]) including also additional points provided kindly by the authors of Ref. [50]. Magenta circles: Our DMRG data (for more details see also Fig. 10).

IC coupling using Eqs. (4), (5), and (6). Keeping only the linear IC coupling term in the expression (6) for $h_{s,2}$, we find

$$\begin{aligned} |J_{0,cr1}^{\text{IC}}| &= \frac{1}{N_{\text{IC}}} \left(\frac{\Delta_1^2}{\Delta_1 + \alpha} - \frac{1}{4\alpha} \right) \\ &= \frac{4\alpha\Delta_1^2 - \Delta_1 - \alpha}{4\alpha(\Delta_1 + \alpha)N_{\text{IC}}} \end{aligned} \quad (9)$$

[cf. also Eq. (51) in Ref. [15], where a bond-operator formalism and a system of vertex equations (BOFVE) is used and where the IC coupling is treated as a small perturbation, only]. Measuring the critical IC coupling in units of J_2 , i.e., considering $J_{0,cr1}^{\text{IC}}/\alpha \equiv \kappa J_{0,cr1}^{\text{IC}}$ as in Fig. 4 and in Ref. [50], one finds in the first-order approximation for the isotropic case a maximum of $\kappa J_{0,cr1}^{\text{IC}} = \frac{3}{4N_{\text{IC}}}(2 - \sqrt{3}) \approx 0.3481/N_{\text{IC}}$ at $\kappa = \sqrt{3}$. The explicit form of Eq. (9) provides also direct qualitative insight into the influence of the exchange anisotropy Δ_1 on the stability of the nematic phase. For $\alpha \gtrsim 0.367$, where

for the isotropic 1D model the nematic phase exists, $|J_{0,cr1}^{\text{IC}}|$ increases with growing Δ_1 ; i.e., an easy-axis anisotropy is in favor of the nematic phase.

Very accurate analytic expression for the critical IC coupling may be obtained by the following straightforward calculation: After substitution of the approximate expression (6) for $h_{s,2}$ into Eq. (4) we write the equation for the determination of the critical IC coupling $J_{0,cr}^{\text{IC}}$ in the form

$$f(J_{0,cr}^{\text{IC}}) = 0, \quad (10)$$

$$f(x) = \eta_4 x^4 + \eta_2 x^2 - \frac{1}{2}(x - J_{0,cr1}^{\text{IC}}). \quad (11)$$

We search the roots of Eq. (10) in the form

$$J_{0,cr2}^{\text{IC}} = J_{0,cr1}^{\text{IC}} + \delta \quad (12)$$

assuming $\delta/J_{0,cr1}^{\text{IC}} \ll 1$. We expand the expression (11) up to the second order,

$$f(J_{0,cr1}^{\text{IC}} + \delta) \approx f + f'\delta + \frac{1}{2}f''\delta^2,$$

where the derivatives and the function f on the right-hand side,

$$f(x) = \eta_4 x^4 + \eta_2 x^2,$$

$$f'(x) = 4\eta_4 x^3 + 2\eta_2 x - \frac{1}{2},$$

$$f''(x) = 12\eta_4 x^2 + 2\eta_2,$$

are taken at $x = J_{0,cr1}^{\text{IC}}$. We then obtain

$$\delta \approx -\frac{2f}{f' - \text{sgn}(f')\sqrt{(f')^2 - 2ff''}}. \quad (13)$$

A comparison of the results of the approximate analytic Eqs. (9), (12), (13), and (14) with the numerical data is shown in Figs. 9 and 10. The deviation of $J_{0,cr2}^{\text{IC}}$ from the numerical solution of the HCB-equations value does not exceed 10^{-3} (3×10^{-5}) for 2D (3D) arrangements of the chains (see Fig. 14 in Appendix B). Thus, Eqs. (12) and (13) provide a tedious but excellent description. In the isotropic 3D case discussed here in detail also the straightforward second-order perturbation theory result yields already a reasonable accuracy but within a much simpler analytical description:

$$|J_{0,cr2}^{\text{IC}}| = \frac{2|J_{0,cr1}^{\text{IC}}|}{1 + \sqrt{1 - 8\eta_2|J_{0,cr1}^{\text{IC}}|}}. \quad (14)$$

In fact, to illustrate this point, we note that the maximum value of $|J_{0,cr}^{\text{IC}}| = 0.0625, 0.702928, 0.07056,$ and 0.0718 (measured in units of $|J_1|$) is achieved at $\alpha_{\text{max}} = 1, 1.06448, 1.07333,$ and about 1.1 within first and second order given by Eqs. (9) and (14), the improved HCB approximation given by Eqs. (12) and (13), and the DMRG result, respectively.

An inspection of the phase diagram shown in Figs. 4 and 9 reveals also that the maximal value for the critical IC coupling J_{cr}^{IC} occurs in the nematic phase at values of $1/\alpha$ near 1.7, i.e., in the region of maximal in-chain frustration and particularly strong quantum fluctuations [32,33]. This can be understood already in linear approximation, where $J_{0,cr1}^{\text{IC}}$ is proportional to the difference of the one- and two-magnon critical fields of an isolated chain $J_{0,cr1}^{\text{IC}} = 2(h_s^{\text{1D}} - h_{s,1}^{\text{1D}})/N_{\text{IC}}$.

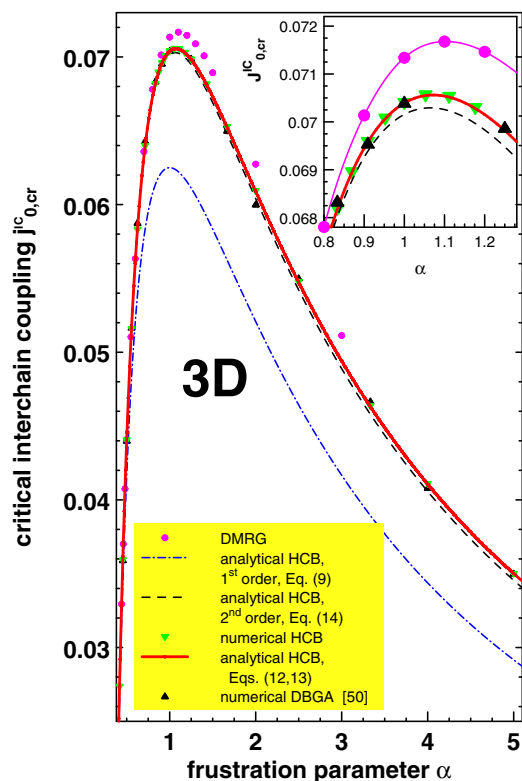


FIG. 10. (Color online) Comparison of the critical IC coupling $J_{0,cr}^{IC}$ as obtained within various methods for the 3D isotropic case of unshifted chains shown on an enlarged scale as compared to the middle curve in Fig. 9 (lower panel). Green triangles show our HCB results and black ones those from the summation of ladder diagrams (Ref. [50]) including also additional points provided kindly by the authors of Ref. [50]. Magenta circles: Our DMRG data. Various analytical HCB based descriptions obtained within the interchain perturbation theory derived in Appendix B are depicted by dashed-dotted (blue), dashed (black), and full (red) lines, respectively, as explained in the legend. Inset: The same for the vicinity of the maximum of $J_{0,cr}^{IC}$.

Finally, we note that the comparison with the results of the summation of ladder diagrams in the dilute Bose gas approximation [50] with one excited “quasiparticle” yields in the 3D case with an accuracy of about 10^{-4} to 10^{-5} the same result as the numerical solution of our HCB equations. This is similar to the pure 1D case (where simple fully analytical expressions are available) as mentioned already in our previous work [32]. In this context it should be noted that the related accuracy problem occurs at two different levels: on a fundamental one concerning the accuracy (validity “in principle”) of the derived basic equations and approaches, and on a purely numerical one related to the solution of the corresponding equations including the determination of the critical IC coupling from Eq. (4) for a given set of Hamiltonian parameters.

A closer inspection of the critical IC couplings $J_{0,cr}^{IC}$ as obtained by the various methods employed here and in the literature [50] is shown in Fig. 10. Starting from about $\alpha \approx 0.9$ one observes systematically slightly larger values for $J_{0,cr}^{IC}$ of our DMRG data as compared to our numerical and analytical

HCB results as well as to the results obtained within the dilute Bose gas approximation [50]. Similar effects occur also in the 2D case (not shown here). The exact reasons for this small difference being mainly of academic theoretical interest remains unclear at present. Its elucidation is beyond the scope of the present paper and therefore postponed to future investigations. The fundamental point is related to the obvious fact that the excitation energy was derived under the assumption of a unique, i.e., nondegenerate, simple ground state given by the fully aligned FM ground state. However, at the critical point we arrive at a situation where the new ground state becomes suddenly degenerate due to the calculated zero excitation energy of the magnetic “quasiparticles” under consideration in formal contradiction with the initial assumption. The solution of this puzzle might lead to a small but finite density of *interacting* condensed quasiparticles in contrast with the single quasiparticles moving in the studied HCB approaches in an effective potential, only (see Appendix A), which allows an exact (closed) solution within the subspaces of one- and two-particle excitations. Anyhow, in our opinion a self-consistent solution of this interesting puzzle seems to be not relevant for the general physical phenomenon considered in the present paper: the detrimental effect of a too strong IC coupling for the realization of MP states in many real 2D and 3D materials.

B. Skew interchain coupling

In the present subsection we consider briefly also the two simplest cases of skew IC couplings for shifted and unshifted nearest-neighboring chains [see Figs. 1(c) and 1(d)], which are relevant for several real edge-shared chain compounds to be discussed below. We apply the same methods as in the previous subsection and restrict ourselves to numerical results, only. The inspection of Fig. 11 reveals that the general behavior is similar to that for perpendicular IC coupling; cf. Fig. 4.

The largest IC coupling that does not destroy the nematic phase again is found for $1/\alpha \equiv |J_1|/J_2 \sim 1.5$ to 2, i.e., in the region of strong in-chain frustration where the quantum

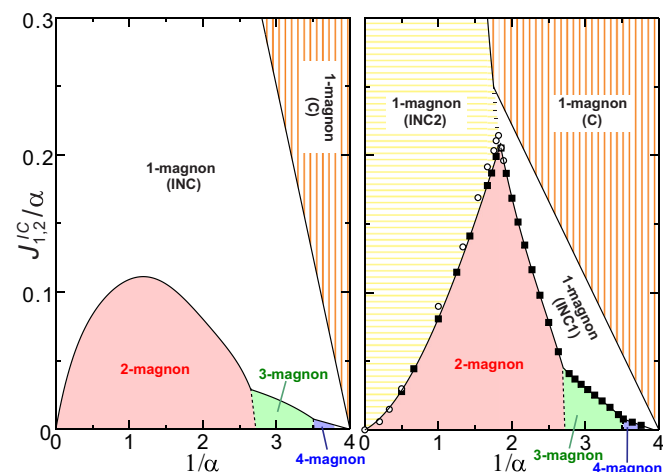


FIG. 11. (Color online) Phase diagram for multipolar phases with skew (diagonal) IC coupling J_1^{IC} (left) and J_2^{IC} (right) in 3D; cf. also Figs. 1(c) and 1(d), respectively. Filled black squares (open circles): DMRG(HCB) results, respectively.

fluctuations are at maximum [32,33]. Approaching the critical point $\alpha = 1/4$ the same sequence of higher multipolar phases is observed. Near the critical point ($\alpha \gtrsim 1/4$) and for almost decoupled Heisenberg chains ($1/\alpha \rightarrow 0$) the saturation field tends to the simple 1-magnon value and additional quantum effects vanish. In the general case, i.e., if both perpendicular and skew IC couplings are present, qualitatively the same behavior in a naturally more complex and extended IC parameter space can be expected. The numerical study of the general case is straightforward using our DMRG approach, but it is left for future studies of concrete materials, if needed.

For completeness we mention here that the stability of the nematic phase for unshifted chains and weak ferromagnetic skew IC coupling has been considered up to the second order in Ref. [15]. The critical IC coupling has been derived therein adopting the validity of Eq. (4), i.e., the competition between the nematic and the dipolar one-magnon phase. However, according to our numerical DMRG results this is not justified in the present case for any pure skew FM IC coupling, because for this situation it is determined by the competition of the nematic phase with higher order multimagnon phases being beyond the range of the present day forms of the HCB and the more approximate low-order IC approach employed in Ref. [50]. Then analogously to Eq. (4) other phases and border lines and/or additional interactions must be examined. We plan to return to this important and challenging issue devoted to a correct microscopic description of LiVCuO₄ in the near future in detail. Here we restrict ourselves to the statement that the claimed reached “reasonable” description of LiVCuO₄ in Appendix B of Ref. [50] in terms of the classical spin-wave-based parameter set proposed in Ref. [14] is not conclusive. What remains is simply the fact that at a weak IC coupling various different 1D parameter sets describe roughly the experimental saturation field data. Hence, in such a situation other properties must be considered to extract the relevant microscopic parameters [33,51].

It is obvious that for shifted chains the region of the nematic phase in the phase diagram exhibits a relatively sharp maximum (peak). Moreover, for shifted chains, the phase diagram becomes more complex due to the presence of *three* one-magnon phases, namely two incommensurate INC1 and INC2 and one commensurate C one-magnon phase. The latter commensurate C phase has been considered in detail in our previous paper [31] devoted to one-magnon peculiarities of the saturation field of Li₂CuO₂. Interestingly, the sharp maximum in the nematic phase corresponds to a triple point, where the two incommensurate one-magnon phases INC1 and INC2 and the nematic phase meet. As a consequence, the border lines with the neighboring incommensurate one-magnon phases exhibit opposite curvatures as compared with the case of unshifted chains. Above this maximum there is even another triple point, where the two incommensurate one-magnon phases INC1 and INC2 meet the one-magnon commensurate C phase. Experimentally, the investigation of systems with parameter regimes near these special points in the phase diagram is promising and might be provide deeper insight into the involved microscopic exchange mechanism. We will discuss this issue in the next section.

IV. DISCUSSION

Having investigated theoretically in general how the competition between frustration, different types of IC coupling, and exchange anisotropy plays out, we now apply these insights to identify candidate materials potentially displaying a quantum MPP. Li₂CuO₂ is near the critical point, having $\alpha \approx 0.33$ and a rather small $\Delta_1 - 1 \approx 0.01$ [30]. Its skew IC coupling J_2^{IC} , see Fig. 1(d), however, is strong enough to even destabilize the spiral state and drives the chains into a state with FM in-chain correlations. Also Li₂ZrCuO₄ is close to the critical point [22] ($\alpha \approx 0.3$) but in this case as well for any realistic IC interaction and reasonable value for Δ_1 , all higher MPP are unstable. The compounds Li(Na)Cu₂O₂ are away from the detrimental critical point but their IC coupling is too large [52–54] ($J^{\text{IC}} \sim 0.5$ to 1) to establish a nematic phase for the estimated, moderate, values of Δ_1 [55].

Instead LiVCuO₄ is a good material for a nematic phase, having a coupling between the chains that is characterized by a very weak J_0^{IC} , which manifests itself in strong quantum fluctuations evidenced by a small ordered magnetic moment ($0.3\mu_B$) at low temperature and the observation of a 2-spinon continuum in inelastic neutron scattering [56]. The weak J^{IC} is also in accord with the fact that its saturation field is close to the value of the uncoupled 1D chain given by h_s^{1D} [51]. In addition, the estimated $\alpha \approx 0.75$ [33,51] near the maximum of the critical $J_{0,\text{cr}}^{\text{IC}}(1/\alpha)$ curve is almost optimal for a nematic phase to survive (see Fig. 4). From a more rigorous quantitative point of view the details of the IC coupling remain still somewhat unclear, since its determination in the region of strong quantum fluctuations is a very difficult task that is clearly beyond the predictions of the standard spin-wave theory nevertheless used in the interpretation of the experimental inelastic neutron scattering data in Ref. [17] and the adopted corresponding results in the saturation field analysis given in Ref. [15].

A very interesting case is provided by the natural mineral linarite, PbCuSO₄(OH)₂, which consists of neutral edge-shared Cu(OH)₂ chains surrounded by Pb²⁺ and [SO₄]^{−2} ions and has $\alpha \approx 0.36$ [26]. Below 2.7 K a spiral state with a pitch angle of 34° sets in [27,57]. A perpendicular J_0^{IC} barely affects the pitch angle of the magnetic spiral, in sharp contrast to skew IC coupling J_1^{IC} . (Without such a realistic skew coupling suggested also by LSDA+*U* based calculations, the pitch would be about twice as large [33], in conflict with the experimental data mentioned above.) We have considered this situation theoretically in more detail and have calculated the phase diagram as a function of (small) anisotropy $\Delta_1 - 1$ and IC coupling J_1^{IC} ; see Fig. 12 [58]. For the given value of α even relatively small values of J_1^{IC} and $\Delta_1 - 1$ are nevertheless sufficient to reduce the pitch from about 60° to the experimental value of 34° obtained from diffraction data collected at a finite low temperature of $T = 1.8$ K but estimated in our present approach at $T = 0$. The experimental pitch strongly restricts the possible values for J_1^{IC} and $\Delta_1 - 1$ (see the red line in Fig. 12). An additional piece of information is the experimental value of the saturation field of about 11 T—the 1D saturation field gives in this case about 5 T—which indicates a reduced value of J_1^{IC} , renormalized by a sizable $\Delta_1 - 1$, placing the system close to the triatic (i.e., the bound three-magnon phase) region of the phase diagram in Fig. 12.

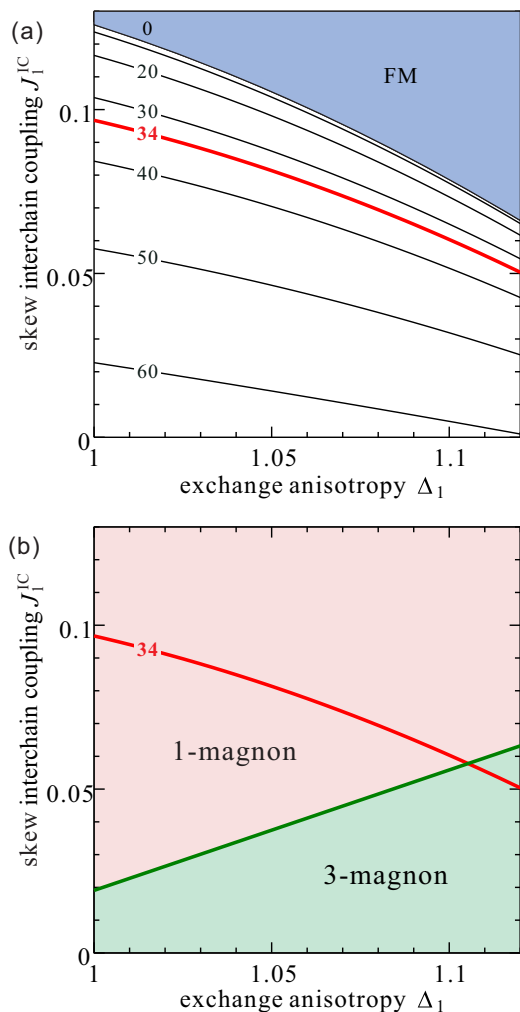


FIG. 12. (Color online) Influence of the first skew interchain coupling J_1^{IC} and an easy-axis anisotropy Δ_1 of the NN exchange coupling on the ground state of a system of coupled anisotropic J_1 - J_2 spin chains for $J_1 = -1$ and an intrachain frustration rate $\alpha = -J_2/J_1 = 0.36$. Panel (a): Zero-field plot of the interchain coupling J_1^{IC} vs easy-axis anisotropy $\Delta_1 > 1$ for various fixed pitch angles ϕ (given in degrees at the left side of each curve). The NNN coupling J_2 is assumed to be isotropic. The ground-state phase with purely FM in-chain correlations (i.e., $\phi = 0$), present for large enough J_1^{IC} , is shown in the light blue upper part of the figure. Note that the red curve corresponds to the experimentally observed pitch angle for $\text{PbCuSO}_4(\text{OH})_2$ (linarite). Panel (b): Character of the lowest excitations above the FM ground state for large external field above the saturation field applied in the easy-axis **b** direction.

In this context experimental studies under chemical or physical pressure are of great interest, since these can significantly change the IC coupling. When applying hydrostatic pressure one expects an increase of the IC coupling and thereby a weakening and possibly disappearance of the MPPs in the mentioned two candidate materials. Vice versa, growing isomorphic crystals with larger isovalent cations (chemical pressure) the interchain coupling can be modified and most probably might be somewhat suppressed. Thus, substituting, e.g., Li by Na, Rb, or Cs, i.e., synthesizing for instance RbCu_2O_2 or CsCu_2O_2 , it is expected to create candidate MPP

materials due to a decrease of the detrimental IC couplings. In other words, if it were possible to synthesize such (hypothetical) compounds, one would expect, e.g., for $\text{Cs}(\text{Rb})\text{Cu}_2\text{O}_2$ and $\text{Na}(\text{Rb})_2\text{ZrCuO}_4$ an increased stability of the nematic and triatic phases, respectively. Using mixed crystals with isovalent partial substitution such as $\text{Li}_{1-x}\text{Na}_x\text{VCuO}_4$ the interchain coupling might be tuned continuously providing this way more insight into its role for different physical properties. Preparing strained epitaxial thin films from candidate materials will allow us to study similar effects, where tuning of the strain by using different substrates can change the IC in different directions.

In view of the ongoing debate on the possibility of a Bose condensation of MP states in 2D or 3D quasi-1D systems and the experimental search in real systems [40,41,43,59,60], we briefly discuss on a qualitative level some consequences, relations, and remaining open questions with respect to the results presented here. First of all, our approach deals with the lowest excitation energy of a single “quasiparticle” for the given simple aligned ground state at the saturation field by a single MP state as compared to the corresponding one-magnon state. Then for slightly lower fields the density of MP states might increase up to a critical value, where the corresponding Bose-Einstein condensation sets in. In other words one starts with a second-order phase transition regarding the density of MP states as a field-dependent order parameter. In this case a too strong IC coupling seems to prevent also a spontaneous creation of a single MP bound state and any Bose-Einstein condensation of several of them at slightly lower fields, too. Due to the more complex ground state of slightly misaligned momenta a rigorous theoretical proof of this intuitive picture, e.g., in terms of the HCB approach employed here, is a challenging many-body problem left for future investigations. Furthermore, the present theory cannot describe the case of a first-order transition, when a finite density of interacting MP states is formed spontaneously at the saturation field. The most challenging and difficult problem for the presently known candidate materials is the theoretical determination of the border line between the SDW_p phases and the corresponding MP phases or the elucidation for the conditions for a spatially homogeneous coexistence/field-driven spatially inhomogeneous phase separation of them [39] within effective models for coupled quasi-1D chain [59] or planar units [61].

Another somewhat unclear question concerns the role of the IC in the formation of a macroscopic condensate in a quasi-1D system with 2D or 3D IC. In spite of the slightly reduced binding energy (cf. the discussion above), there must be nevertheless also tunneling processes (provided by the same interactions) between the chains in order to perform the corresponding 2D or 3D ground state. Probably, a very weak IC well below the critical coupling strength considered in Sec. III is sufficient to establish the corresponding ordering like in quasi-low-dimensional superconductors provided by the Josephson coupling of planes or chains.

V. SUMMARY

We have demonstrated the crucial role of different types of antiferromagnetic and ferromagnetic interchain interactions and of a uniaxial exchange anisotropy for the NN in-chain exchange in frustrated quasi-1D helimagnets. The anisotropy

of the NNN in-chain does not affect the stability of multipolar states in the adopted simple easy-axis case. The rich and exotic physics of multipolar phases recently predicted for single chains is very sensitive to the strength and type of the additional interchain interactions unavoidable in real compounds as well as to the frequently observed easy-axis anisotropy of the NN in-chain coupling.

The investigations of the present paper are representative for a number of spin- $\frac{1}{2}$ quasi-1D frustrated helimagnetic materials but still not fully comprehensive. Indeed, more complex forms of the interchain couplings, in-chain exchange, and alternation, as well as other cases of symmetric and antisymmetric exchange patterns, can be present and relevant in real compounds and merit systematic investigation. Also impurities always present in real materials can affect the physical properties significantly, especially for LiVCuO₄ in which some Li ions can be misplaced on Cu sites and vice versa; also these effects are worth studying in detail microscopically.

ACKNOWLEDGMENTS

We thank H. Ueda for providing us with published and unpublished data included in Fig. 9, and H. Rosner, A. U. B. Wolter, and M. Schäpers for discussions on linarite. This work is supported by SFB 1143 of the Deutsche Forschungsgemeinschaft.

APPENDIX A: EXACT TWO-MAGNON GREEN'S FUNCTION

At high magnetic fields, the Hamiltonian of coupled frustrated spin- $\frac{1}{2}$ J_1 - J_2 XXZ-Heisenberg chains reads

$$\hat{H} = \hat{H}_{1D} + \hat{H}_{IC}, \quad (\text{A1})$$

$$\hat{H}_{1D} = \sum_{\mathbf{m}} \left[\frac{1}{2} \sum_{\mathbf{n}} J_{\mathbf{n}} (\Delta_{\mathbf{n}} \hat{S}_{\mathbf{m}}^z \hat{S}_{\mathbf{m}+\mathbf{n}}^z + \hat{S}_{\mathbf{m}}^+ \hat{S}_{\mathbf{m}+\mathbf{n}}^-) - h \hat{S}_{\mathbf{m}}^z \right], \quad (\text{A2})$$

$$\hat{H}_{IC} = \frac{1}{2} \sum_{\mathbf{m}, \mathbf{f}} J_{\mathbf{f}} [\Delta_{\mathbf{f}} \hat{S}_{\mathbf{m}}^z \hat{S}_{\mathbf{m}+\mathbf{f}}^z + \hat{S}_{\mathbf{m}}^+ \hat{S}_{\mathbf{m}+\mathbf{f}}^-], \quad (\text{A3})$$

where \mathbf{m} enumerates the lattice sites, $\mathbf{n} = \pm \mathbf{n}\mathbf{a}$, $n = 1, 2$ determines the NN sites within the chain, and \mathbf{a} is the lattice vector along the chain. The vector \mathbf{f} connects sites at different chains. For the sake of convenience we set and denote for the two in-chain couplings $J_1 \equiv -1$ (FM) and $J_2 = \alpha > 0$ (AFM), respectively. The Hamiltonian given by Eq. (A1) is more general than that from Eq. (1); it allows for uniaxial anisotropy of all exchange couplings. The magnetic field is directed along the anisotropy axis.

In terms of hard-core boson operators b , defined by

$$\begin{aligned} \hat{S}^+ &\equiv b, & \hat{S}^- &\equiv b^\dagger, & \hat{S}^z &\equiv \frac{1}{2} - \hat{n}, \\ \hat{n}_{\mathbf{m}} &= b_{\mathbf{m}}^\dagger b_{\mathbf{m}} = 0, 1, \\ \{b_{\mathbf{m}}, b_{\mathbf{m}}^\dagger\} &= 1, & [b_{\mathbf{m}}, b_{\mathbf{m}'}^\dagger] &= 0, & \mathbf{m} &\neq \mathbf{m}', \\ b_{\mathbf{m}}^\dagger |FM\rangle &\equiv b_{\mathbf{m}}^\dagger |\cdots \uparrow \uparrow \uparrow \mathbf{m} \uparrow \uparrow \uparrow \cdots\rangle \\ &= |\cdots \uparrow \uparrow \downarrow_{\mathbf{m}} \uparrow \uparrow \uparrow \cdots\rangle, \\ (b_{\mathbf{m}}^\dagger)^2 &= (b_{\mathbf{m}})^2 = 0, \end{aligned} \quad (\text{A4})$$

the Hamiltonian (A1) becomes

$$\hat{H} = \hat{H}_0 + \hat{H}_{\text{int}}, \quad (\text{A5})$$

$$\hat{H}_0 = \omega_0 \sum_{\mathbf{m}} \hat{n}_{\mathbf{m}} + \frac{1}{2} \sum_{\mathbf{m}, \mathbf{R}} J_{\mathbf{R}} b_{\mathbf{m}}^\dagger b_{\mathbf{m}+\mathbf{R}}, \quad (\text{A6})$$

$$\hat{H}_{\text{int}} = \frac{1}{2} \sum_{\mathbf{m}, \mathbf{R}} J_{\mathbf{R}} \Delta_{\mathbf{R}} \hat{n}_{\mathbf{m}} \hat{n}_{\mathbf{m}+\mathbf{R}}, \quad (\text{A7})$$

where $\omega_0 \equiv h - \frac{1}{2} \sum_{\mathbf{R}} J_{\mathbf{R}} \Delta_{\mathbf{R}}$, $\mathbf{R} = \mathbf{n}, \mathbf{f}$.

The n -particle excitation spectra are given by the singularities of the corresponding retarded Green's functions (GFs):

$$\langle\langle \hat{X} | \hat{Y} \rangle\rangle \equiv -i \int_{t'}^{\infty} dt e^{i\omega(t-t')} \langle [\hat{X}(t), \hat{Y}(t')] \rangle, \quad (\text{A8})$$

$$\omega \langle\langle \hat{X} | \hat{Y} \rangle\rangle = \langle [\hat{X}, \hat{Y}] \rangle + \langle\langle [\hat{X}, \hat{H}] | \hat{Y} \rangle\rangle. \quad (\text{A9})$$

A negative (zero) value of the excitation energy signals an instability of the ground state, which is given by the fully polarized state achieved from below for a magnetic field first at the saturation field $h = h_s$. The equation of motion for the two-magnon operator,

$$\hat{A}_{\mathbf{k},1} = \frac{1}{\sqrt{N}} \sum_{\mathbf{m}} e^{-i\mathbf{k}(\mathbf{m}+1/2)} b_{\mathbf{m}} b_{\mathbf{m}+1} = \hat{A}_{\mathbf{k},-1}, \quad (\text{A10})$$

reads

$$\begin{aligned} [\hat{A}_{\mathbf{k},1}, \hat{H}] &= \left(2\omega_0 + \sum_{\mathbf{R}} J_{\mathbf{R}} \Delta_{\mathbf{R}} \delta_{\mathbf{l},\mathbf{R}} \right) \hat{A}_{\mathbf{k},1} \\ &+ (1 - \delta_{\mathbf{l},0}) \sum_{\mathbf{R}} J_{\mathbf{R}} \cos \frac{\mathbf{k}\mathbf{R}}{2} \hat{A}_{\mathbf{k},1+\mathbf{R}}, \end{aligned} \quad (\text{A11})$$

where \mathbf{k} is the total quasimomentum of the magnon pair, $N = N_{\perp} N_x$ is the number of sites, N_{\perp} is the number of chains, and N_x denotes the number of sites in the chain.

As usual, the exclusion of the center-of-mass motion reduces the problem of an interacting pair of particles to a one-particle problem of motion in an effective potential well. In our case it corresponds to an impurity problem in a tight-binding Hamiltonian [32] (see Fig. 13)

$$\hat{H}_{tb}(\mathbf{k}) = \hat{T}(\mathbf{k}) + \hat{V}, \quad (\text{A12})$$

$$\hat{T}(\mathbf{k}) = 2\omega_0 \sum_{\mathbf{m}} |\mathbf{m}\rangle \langle \mathbf{m}| + \sum_{\mathbf{m}, \mathbf{R}} |\mathbf{m} + \mathbf{R}\rangle t_{\mathbf{R}}(\mathbf{k}) \langle \mathbf{m}|, \quad (\text{A13})$$

$$\hat{V} = \sum_{\mathbf{m}'} |\mathbf{m}'\rangle \varepsilon_{\mathbf{m}'} \langle \mathbf{m}'|, \quad (\text{A14})$$

where

$$t_{\mathbf{R}}(\mathbf{k}) = J_{\mathbf{R}} \cos \frac{\mathbf{k}\mathbf{R}}{2}, \quad (\text{A15})$$

$$\mathbf{m}' = \mathbf{0}, \mathbf{r}, \mathbf{f}, \varepsilon_0 = \infty, \quad \varepsilon_{\mathbf{R}} = J_{\mathbf{R}} \Delta_{\mathbf{R}}. \quad (\text{A16})$$

The Hamiltonian depends on the total pair momentum.

The two-magnon GF reads

$$G_{\mathbf{l},\mathbf{n}}(\mathbf{k}, \omega) = \langle\langle A_{\mathbf{k},1} | A_{\mathbf{k},\mathbf{n}}^\dagger \rangle\rangle = \langle \phi_{\mathbf{l}} | (\omega - \hat{H}_{tb})^{-1} | \phi_{\mathbf{n}} \rangle, \quad (\text{A17})$$

with $|\phi_{\mathbf{l}}\rangle = (|\mathbf{l}\rangle + |-\mathbf{l}\rangle)/\sqrt{2}$. The GF is analytic everywhere in the complex energy plane but may have singularities on

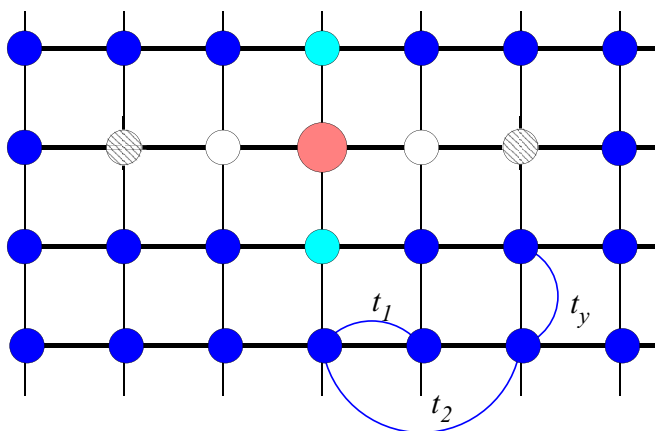


FIG. 13. (Color online) Cartoon of the effective impurity problem given by the Hamiltonian (A12), which describes the internal motion of a magnon pair with the total quasimomentum \mathbf{k} (2D case). The pink, open, shaded, and cyan circles depict the impurities with $\varepsilon_{\mathbf{m}} = \infty, \Delta_1, \alpha, J_0^{\text{IC}}$ (in units of $|J_1|$), respectively. Blue filled circles: the regular sites of the lattice; arcs: the \mathbf{k} -dependent hoppings given by Eq. (A15) (in units of $|J_1|$), i.e., $t_1 = -\cos(\mathbf{k}\mathbf{a}/2)$, $t_2 = \alpha \cos(\mathbf{k}\mathbf{a})$, and $t_y = J_0^{\text{IC}} \cos(\mathbf{k}\mathbf{b}/2)$.

the real axis: branch cuts and isolated poles. The branch cuts correspond to the continuum spectrum of unbounded motion of the effective particle, which in its turn corresponds to the two-particle continuum in the pair motion. The poles correspond to the energies of localized impurity states, which are bound states for the pair when the energies lie below the continuum or anti-bound-states in the opposite case. It is clear from Eqs. (A12)–(A16) that bound states are possible only when some $\varepsilon_{\mathbf{R}}$ are negative, i.e., for FM $J_{\mathbf{R}} < 0$. The bound-state energy $\omega_b(\mathbf{k})$ and the continuum boundaries depend on the total momentum of the pair \mathbf{k} . If the bound-state energy minimum lies below the lowest continuum energy (that may occur at different \mathbf{k} values), the bound pairs will condense at magnetic fields just below the saturation field, the gas of pairs being the nematic state of the magnetic system [7,15].

When all $J_{\mathbf{R}}$ are positive, like in the AFM-AFM J_1 - J_2 model, only anti-bound-states occur at energies higher than the two-particle continuum. In this case only the one-magnon condensation occurs below the saturation field.

We will use the identity

$$\hat{G} = \hat{g} + \hat{g} \hat{V} \hat{G} \quad (\text{A18})$$

for the solution in the real space of the impurity problem given by Eqs. (A12)–(A17) (see Fig. 13). In Eq. (A18), $\hat{g} \equiv (\omega - \hat{T})^{-1}$ is the resolvent operator for the periodic part, and $\hat{G} \equiv (\omega - \hat{H}_{tb})^{-1}$ is the resolvent for the impurity problem. According to Ref. [62], we may solve the problem step by step. Starting from the GF of a free particle, which in matrix form reads

$$g_{\mathbf{l},\mathbf{n}} = g_{\mathbf{l}-\mathbf{n}}(\mathbf{k},\omega) \quad (\text{A19})$$

$$= \frac{1}{N} \sum_{\mathbf{q}} \frac{\cos \mathbf{q}(\mathbf{l} - \mathbf{n})}{\omega - (\omega_{\mathbf{k}/2+\mathbf{q}}^{\text{SW}} + \omega_{\mathbf{k}/2-\mathbf{q}}^{\text{SW}})}, \quad (\text{A20})$$

$$\omega_{\mathbf{q}}^{\text{SW}} = \omega_0 + \frac{1}{2} \sum_{\mathbf{R}} J_{\mathbf{R}} e^{i\mathbf{q}\mathbf{R}}, \quad (\text{A21})$$

we add the impurity at the origin. Its infinite potential reflects the impossibility to have two particles on the same site (A4),

$$g_{\mathbf{l},\mathbf{n}}^{(0)} = g_{\mathbf{l},\mathbf{n}} + g_{\mathbf{l},0} \varepsilon_0 g_{0,\mathbf{n}}^{(0)}, \quad (\text{A22})$$

$$g_{\mathbf{l},\mathbf{n}}^{(0)} = g_{\mathbf{l},\mathbf{n}} + \frac{g_{\mathbf{l},0} \varepsilon_0 g_{0,\mathbf{n}}}{1 - \varepsilon_0 g_{0,0}} \rightarrow g_{\mathbf{l},\mathbf{n}} - \frac{g_{\mathbf{l},0} g_{0,\mathbf{n}}}{g_{0,0}}.$$

Next, we add an impurity at the site \mathbf{i} and express the GF via $\hat{g}^{(0)}$:

$$g_{\mathbf{l},\mathbf{n}}^{(i)} = g_{\mathbf{l},\mathbf{n}}^{(0)} + \frac{g_{\mathbf{l},\mathbf{i}}^{(0)} \varepsilon_i g_{\mathbf{i},\mathbf{n}}^{(0)}}{1 - \varepsilon_i g_{\mathbf{i},\mathbf{i}}^{(0)}},$$

and so on; the GF of the system with r impurities is expressed via the GF of the system with $r - 1$ impurities:

$$g_{\mathbf{l},\mathbf{n}}^{(r)} = g_{\mathbf{l},\mathbf{n}}^{(r-1)} + \frac{g_{\mathbf{l},\mathbf{r}}^{(r-1)} \varepsilon_r g_{\mathbf{r},\mathbf{n}}^{(r-1)}}{1 - \varepsilon_r g_{\mathbf{r},\mathbf{r}}^{(r-1)}}. \quad (\text{A23})$$

Thus, in principle, we may take into account any number of in-chain and interchain exchange couplings (IC) and obtain $G_{\mathbf{l},\mathbf{n}}(\mathbf{k},\omega)$ [Eq. (A17)]. The explicit expression for the GF $G_{\mathbf{l},\mathbf{l}}(k,\omega)$ for the 1D J_1 - J_2 model (2) has been given in Ref. [32]. Its spectral density is plotted in the upper panel of Fig. 3. The sharp \mathbf{k} -dependent peaks below the two-particle continuum corresponds to bound pairs of magnons.

APPENDIX B: PHASE BOUNDARY BETWEEN DIPOLAR AND NEMATIC PHASES

At higher dimensions, the role of the interchain interaction (A3) is twofold. First, the periodic part of the effective Hamiltonian (A13) becomes D -dimensional. This changes \hat{g} from Eq. (A19) via the change of $\omega_{\mathbf{q}}^{\text{SW}}$ (A21). Second, new impurities with the strength $\varepsilon_{\mathbf{f}} = J_{\mathbf{f}} \Delta_{\mathbf{f}}$ are added at points \mathbf{r} . The simplest geometry for the IC corresponds to \mathbf{f} vectors perpendicular to the chains, which connect NN sites, only, $J_{\mathbf{f}} = J_0^{\text{IC}}$. The spectral density for the GF $G_{\mathbf{a},\mathbf{a}}(\mathbf{k},\omega)$ for $\mathbf{k} \parallel \mathbf{a}$ for the 2D case is depicted in the middle panel of Fig. 3. We see that for small IC couplings the spectral density behaves qualitatively similar to the 1D case; i.e., the peak corresponding to a bound pair lies below the continuum, and its dispersion exhibits a minimum at the total momentum $\mathbf{k}\mathbf{a} = \pi$ of a bound pair. We have checked numerically that the minimum position remains at the point $\mathbf{k}_{\pi} = (\pi/a, 0, 0)$ for all values of the IC satisfying the condition $J_0^{\text{IC}} < J_{\text{cr}}$ being the critical IC defined implicitly by Eq. (4). On the lower panel of Fig. 3 we see that the behavior of the spectral density changes for large enough IC. The bound state is still present near the edge of the Brillouin zone, but its energy is higher than the minimum of the two-particle continuum. It is clear that the critical IC value J_{cr} is defined by the condition

$$\omega_b \equiv \omega(\mathbf{k}_{\pi}) = \omega_{\min}, \quad (\text{B1})$$

where $\omega_{\min} = 2(h - h_{s,1})$ is the minimum of the energy of the two-particle continuum, and

$$h_{s,1} \equiv -\Delta_1 + \alpha(\Delta_2 + 1) + 0.125/\alpha + 0.5N_{\text{IC}}(J_0^{\text{IC}} \Delta_{\text{IC}} + |J_0^{\text{IC}}|), \quad (\text{B2})$$

is the critical field of the 1-magnon instability [see Eqs. (B2) and (5)].

In order to find the expression for the saturation field \mathcal{H}_s as a function of the interchain coupling $|J_0^{\text{IC}}| < J_{\text{cr}}$, we need the expression for ω_b , which is the position of an isolated pole of the GF:

$$[G_{\mathbf{a},\mathbf{a}}(\mathbf{k}_\pi, \omega_b)]^{-1} = 0. \quad (\text{B3})$$

In terms of the effective model $\hat{H}_{tb}(\mathbf{k}_\pi)$ (A12), ω_b is the energy of the localized impurity level. From Eq. (A15) we see that the nearest-neighbor hopping along the chain vanishes, $t_{\mathbf{a}} = -\cos \frac{\pi}{2} = 0$, and the sites with $\mathbf{r} = n\mathbf{a} + m\mathbf{b} + l\mathbf{c}$ having odd and even n 's are decoupled. In the subsystem with odd n 's, only two impurities of the same strength $\varepsilon_{\mathbf{a}} = J_1 = -1$ are present at the sites $\pm\mathbf{a} = (\pm a, 0, 0)$. The effective particle motion is not affected either by the impurity at the origin (of infinite strength) or by the impurities at the sites $\pm 2\mathbf{a} = (\pm 2a, 0, 0)$ and $\mathbf{f} = (0, \pm b, 0), (0, 0, \pm c)$ with the energies $\alpha\Delta_2$ and $J_0^{\text{IC}}\Delta_{\text{IC}}$, respectively. Note that this peculiarity has an important consequence: the critical value of the IC given by Eqs. (9) and (12) depends only on the NN exchange anisotropy value Δ_1 and not on the NNN Δ_2 . It explains also why the critical IC coupling value is the same for FM and AFM IC within our approach.

So, we may immediately write down the expression for the GF (cf. Eq. (49) of Ref. [32]):

$$G_{\mathbf{a},\mathbf{a}}(\mathbf{k}_\pi, \omega) = \{[G_{\mathbf{a},\mathbf{a}}^{(0)}(\mathbf{k}_\pi, \omega)]^{-1} - J_1\Delta_1\}^{-1}, \quad (\text{B4})$$

where

$$\begin{aligned} G_{\mathbf{a},\mathbf{a}}^{(0)}(\mathbf{k}_\pi, \omega) &= \langle \phi_{\mathbf{a}} | (\omega - \hat{T}(\mathbf{k}_\pi) - |\mathbf{0}\rangle\varepsilon_0|\mathbf{0}\rangle)^{-1} | \phi_{\mathbf{a}} \rangle \\ &= g_0(\mathbf{k}_\pi) + g_{2\mathbf{a}}(\mathbf{k}_\pi) - \frac{2g_{\mathbf{a}}^2(\mathbf{k}_\pi)}{g_0} \end{aligned} \quad (\text{B5})$$

$$= g_0(\mathbf{k}_\pi) + g_{2\mathbf{a}}(\mathbf{k}_\pi). \quad (\text{B6})$$

In Eq. (B5) we have used the relation (A22) and Eq. (B6) which follows from $g_{\mathbf{a}}(\mathbf{k}_\pi) = 0$, since the vector \mathbf{a} joins two decoupled subsystems. Then Eq. (B3) may be rewritten as

$$G_{\mathbf{a},\mathbf{a}}^{(0)}(\mathbf{k}_\pi, \omega) = (J_1\Delta_1)^{-1} = -1/\Delta_1. \quad (\text{B7})$$

Now, using the definition (A19), we may write

$$G_{\mathbf{a},\mathbf{a}}^{(0)}(\mathbf{k}_\pi, \omega) = \frac{1}{N_\perp} \sum_{q_y, q_z} G_{1,1}^{(0)}(\pi, \omega - E_\perp(\pi, \mathbf{q})), \quad (\text{B8})$$

$$G_{1,1}^{(0)}(\pi, \omega) = \frac{1}{N_x} \sum_{q_x} \frac{1 + \cos 2q_x a}{\omega - E_{1D}(\pi, q_x)}, \quad (\text{B9})$$

$$E_{1D}(\pi, q_x) = 2[h + \Delta_1 - \alpha(\cos 2q_x a + \Delta_2)], \quad (\text{B10})$$

$$E_\perp(\pi, \mathbf{q}) = N_{\text{IC}} J_0^{\text{IC}} (\gamma_{\mathbf{q}} - \Delta_{\text{IC}}), \quad (\text{B11})$$

where $\gamma_{\mathbf{q}} = \cos q_y b + (\cos q_y b + \cos q_z c)/2$, $N_{\text{IC}} = 2$ (4) for a 2D (3D) geometry. In the 2D case the summation over q_z should be dropped. The 1D GF as given by Eq. (B9) is easily calculated:

$$G_{1,1}^{(0)}(\pi, \omega) = G(z)/\alpha, \quad (\text{B12})$$

$$G(z) = [z + 1 - \tau(z)]^{-1}, \quad (\text{B13})$$

where

$$z(\omega) \equiv [\omega - 2(h + \Delta_1 - \alpha\Delta_2)]/\alpha, \quad (\text{B14})$$

and the dimensionless Green's function of a semi-infinite tight-binding chain $\tau(z) = [z - \tau(z)]^{-1}$. Now, we search for the solution of Eq. (B4) in the form

$$\omega_b = \alpha(z_{b1} + \zeta) + 2(h + \Delta_1 - \alpha\Delta_2 - \frac{1}{2}N_{\text{IC}}J_0^{\text{IC}}\Delta_{\text{IC}}), \quad (\text{B15})$$

where ζ is unknown, and

$$z_{b1} \equiv -\left(\frac{\Delta_1 + \alpha}{\alpha} + \frac{\alpha}{\Delta_1 + \alpha}\right) \quad (\text{B16})$$

is the solution for the 1D problem [32]. Note that in the present work we use another definition for the frustration parameter $\alpha \equiv J_2/|J_1|$ as compared to Ref. [32].

Assuming $\zeta \ll 1$, we rewrite Eq. (B7) in the form

$$\frac{1}{N_\perp} \sum_{q_y, q_z} \sum_{m=0}^{\infty} \frac{G^{(m)}}{m!} (\zeta - e_{\mathbf{q}})^m = -\frac{\alpha}{\Delta_1}, \quad (\text{B17})$$

where $e_{\mathbf{q}} \equiv N_{\text{IC}} J_0^{\text{IC}} \gamma_{\mathbf{q}}/\alpha$,

$$G^{(m)} \equiv \left(\frac{\partial}{\partial z}\right)^m G(z) |_{z=z_{b1}}. \quad (\text{B18})$$

Note that $G(z_{b1}) = -\alpha/\Delta_1$, and keeping only terms with $m \leq 4$, we obtain the equation

$$\begin{aligned} \zeta G' + \frac{1}{2}(\zeta^2 + \overline{e_{\mathbf{q}}^2})G'' + \frac{1}{6}(\zeta^3 + 3\zeta\overline{e_{\mathbf{q}}^2})G''' \\ + \frac{1}{24}(\zeta^4 + 6\zeta^2\overline{e_{\mathbf{q}}^2} + \overline{e_{\mathbf{q}}^4})G^{IV} = 0, \end{aligned} \quad (\text{B19})$$

where

$$\overline{e_{\mathbf{q}}^m} \equiv \frac{1}{N_\perp} \sum_{q_y, q_z} e_{\mathbf{q}}^m, \quad (\text{B20})$$

and we have taken into account that $\overline{e_{\mathbf{q}}^m} = \overline{e_{\mathbf{q}}^{2n-1}} = 0$ after a direct calculation, whereas for even $m = 2n$ substituting the expression of $\gamma_{\mathbf{q}}$, we obtain

$$\begin{aligned} \overline{e_{\mathbf{q}}^{2n}} &= \left(\frac{N_{\text{IC}}J_0^{\text{IC}}}{\alpha}\right)^{2n} \frac{1}{\pi} \int_0^\pi \cos^{2n} x dx, \\ &= \left(\frac{J_0^{\text{IC}}}{\alpha}\right)^{2n} \frac{2^n(2n-1)!!}{n!} \quad \text{for 2D}; \quad (\text{B21}) \\ \overline{e_{\mathbf{q}}^{2n}} &= \left(\frac{N_{\text{IC}}J_0^{\text{IC}}}{2\alpha}\right)^{2n} \left(\frac{1}{2\pi}\right)^2 \iint_{-\pi}^\pi (\cos x + \cos y)^{2n} dx dy, \end{aligned} \quad (\text{B22})$$

for 3D. Notice that for both 2D and 3D cases

$$\overline{e_{\mathbf{q}}^2} = N_{\text{IC}}(J_0^{\text{IC}}/\alpha)^2$$

holds. For the next term $m = 4$ we have

$$\begin{aligned} \overline{e_{\mathbf{q}}^4} &= \left(\frac{2J_0^{\text{IC}}}{\alpha}\right)^4 \frac{1}{16\pi} \int_{-\pi}^\pi (\cos 4x + 4\cos 2x + 3) dx \\ &= \frac{3}{8} \left(\frac{2J_0^{\text{IC}}}{\alpha}\right)^4 \end{aligned} \quad (\text{B23})$$

for 2D, and

$$\begin{aligned} \overline{e_q^4} &= \left(\frac{2J_0^{\text{IC}}}{\alpha}\right)^4 \left[\frac{1}{\pi} \int_{-\pi}^{\pi} \cos^4 x dx + \frac{3}{2\pi^2} \left(\int_{-\pi}^{\pi} \cos^2 x dx \right)^2 \right] \\ &= \frac{9}{4} \left(\frac{2J_0^{\text{IC}}}{\alpha}\right)^4 \end{aligned} \quad (\text{B24})$$

for 3D. We see that starting with $n = 4$ the role of the space dimension cannot be reduced to the number of neighbors N_{IC} , and the topology of interaction bonds comes into play. We will see below that this leads to the difference between 2D and 3D values of η_4 :

$$G' = G^2[\tau' - 1], \quad (\text{B25})$$

$$G'' = 2G^3[\tau' - 1]^2 + G^2\tau'', \quad (\text{B26})$$

$$G''' = 6G^4[\tau' - 1]^3 + 6G^3[\tau' - 1]\tau'' + G^2\tau''', \quad (\text{B27})$$

$$\begin{aligned} G^{IV} &= 24G^5[\tau' - 1]^4 + 36G^4[\tau' - 1]^2\tau'' \\ &+ 6G^3(\tau'')^2 + 8G^3[\tau' - 1]\tau''' + G^2\tau^{IV}, \end{aligned} \quad (\text{B28})$$

$$\tau' = -\frac{\alpha^2}{\Delta_1(\Delta_1 + 2\alpha)},$$

$$\tau'' = -2\left[\frac{\alpha(\Delta_1 + \alpha)}{\Delta_1(\Delta_1 + 2\alpha)}\right]^3,$$

$$\tau''' = -6\left[\frac{\alpha(\Delta_1 + \alpha)}{\Delta_1(\Delta_1 + 2\alpha)}\right]^4 \frac{\Delta_1^2 + 2\Delta_1\alpha + 2\alpha^2}{\Delta_1(\Delta_1 + 2\alpha)},$$

$$\tau^{IV} = -24\frac{\alpha^5(\Delta_1 + \alpha)^5 F}{[\Delta_1(\Delta_1 + 2\alpha)]^7},$$

$$F \equiv \Delta_1^4 + 4\Delta_1^3\alpha + 9\Delta_1^2\alpha^2 + 10\Delta_1\alpha^3 + 5\alpha^4.$$

Substituting the expansion

$$\zeta = \zeta_1 J_0^{\text{IC}} + \zeta_2 (J_0^{\text{IC}})^2 + \zeta_3 (J_0^{\text{IC}})^3 + \zeta_4 (J_0^{\text{IC}})^4 \quad (\text{B29})$$

into Eq. (B19), we obtain

$$\zeta_1 = \zeta_3 = 0, \quad (\text{B30})$$

$$\begin{aligned} \zeta_2 &= -\frac{N_{\text{IC}}G''}{2\alpha^2G'} \\ &= -\frac{N_{\text{IC}}(\Delta_1 + \alpha)}{\alpha[\Delta_1(\Delta_1 + 2\alpha)]^2} [\Delta_1^2 + 3\Delta_1\alpha + 3\alpha^2], \end{aligned} \quad (\text{B31})$$

$$\zeta_4 = -\frac{1}{G'} \left[\frac{G''}{2} \zeta_2^2 + \frac{N_{\text{IC}}G'''}{2\alpha^2} \zeta_2 + \frac{G^{IV}}{24(J_0^{\text{IC}})^4} \overline{e_q^4} \right]. \quad (\text{B32})$$

At the saturation field, ω_b in the right-hand side of Eq. (B15) vanishes, and we obtain

$$\begin{aligned} h_{s,2} &= h_{s,2}^{\text{1D}} + \frac{N_{\text{IC}}}{2} J_0^{\text{IC}} \Delta_{\text{IC}} \\ &\quad - \frac{\alpha}{2} [\zeta_2 (J_0^{\text{IC}})^2 + \zeta_4 (J_0^{\text{IC}})^4], \end{aligned} \quad (\text{B33})$$

$$h_{s,2}^{\text{1D}} = -\Delta_1 + \alpha\Delta_2 - \frac{\alpha}{2} z_{b1}.$$

Equation (B33) coincides with Eq. (6) with

$$\eta_i = -0.5\alpha\zeta_i/N_{\text{IC}}. \quad (\text{B34})$$

We see from Eqs. (B31) and (B34) that η_2 does not depend on the dimensionality (or more precisely on the number of interacting NN chains, since a 3D square lattice with $N_{\text{IC}} = 4$ differs in general, e.g., from a hypothetical 3D hexagonal chain lattice with $N_{\text{IC}} = 3$ not considered in the present paper devoted mainly to known typical edge-shared cuprate chains). However, in higher orders, the geometry of exchange paths plays a nontrivial role. The term $\overline{e_q^4}$ (B24) in Eq. (B32) is not simply proportional to N_{IC}^2 as are other terms. It is clear from the definition that $\overline{e_q^m}$ (B20) will have nontrivial dependence on $m > 2$.

The boundary between the 1-magnon and the 2-magnon phases is obtained by solving Eq. (4) for the critical IC $J_{\text{cr}}^{\text{IC}}$. If one retains only the linear term in the expansion in powers of the IC given by (B33), we obtain $|J_{\text{cr},1}^{\text{IC}}|$ given by Eq. (9). This approximation demonstrates the qualitative behavior of $J_{\text{cr}}^{\text{IC}}$ as a function of the anisotropy and the frustration parameters Δ_1 and α , respectively. Practically, a complete quantitative agreement with our numerical data is achieved, if we use

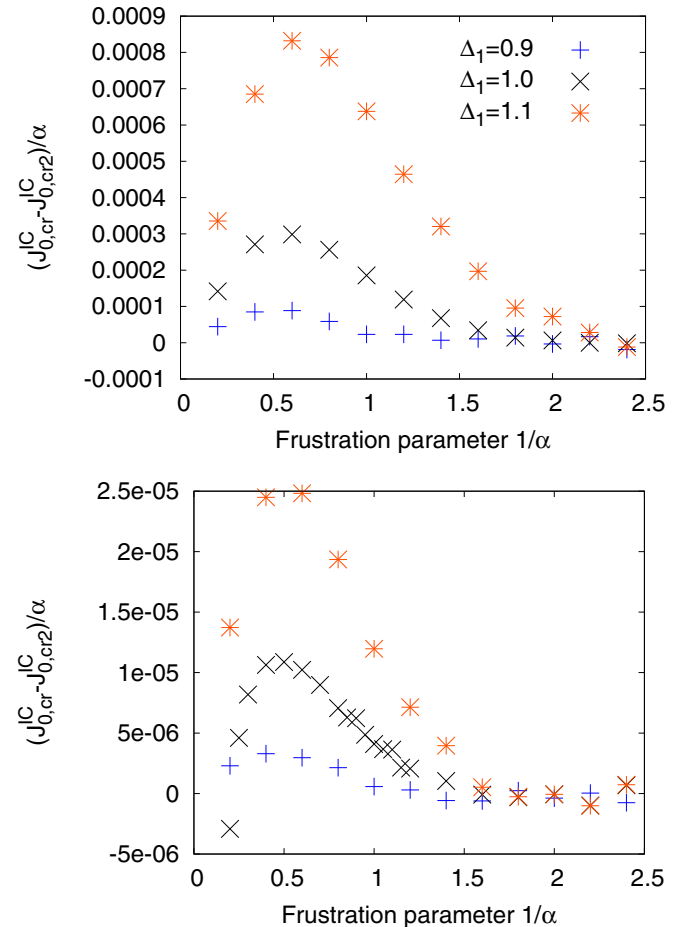


FIG. 14. (Color online) Difference between the numerical solution of the HCB Eq. (B3) and the implicit analytic expression given by Eqs. (12) and (13) (see Fig. 9). The upper (lower) panel shows the 2D (3D) case.

Eqs. (12) and (13). The high precision of these expressions is shown in Fig. 14.

It is convenient to normalize the couplings on $J_2 > 0$, and introduce $\kappa \equiv 1/\alpha$, which measures the attraction provided by the FM J_1 . Using the same normalization for the IC, too, we write $y \equiv J_0^{\text{IC}}/\alpha$. Then Eqs. (B31) and (9) may be rewritten

as

$$\zeta_2 = -\frac{N_{\text{IC}}(\kappa\Delta_1 + 1)}{[\Delta_1(\kappa\Delta_1 + 2)]^2} [\kappa^2\Delta_1^2 + 3\Delta_1\kappa + 3], \quad (\text{B35})$$

$$|y_{cr,1}| = \frac{\kappa^2(4\Delta_1^2 - \kappa\Delta_1 - 1)}{4N_{\text{IC}}(\kappa\Delta_1 + 1)}. \quad (\text{B36})$$

-
- [1] C. Castelnovo, R. Moessner, and S. L. Sondhi, *Nature (London)* **451**, 42 (2008).
- [2] U. Schollwöck, J. Richter, D. Farnell, and R. Bishop (eds.), *Quantum Magnetism*, Lecture Notes in Physics, Vol. 645 (Springer-Verlag, Berlin, 2004).
- [3] C. Lacroix, P. Mendels, and F. Mila (eds.), *Introduction to Frustrated Magnetism* (Springer-Verlag, Berlin, 2011).
- [4] L. Balents and O. A. Starykh, [arXiv:1510.07640](https://arxiv.org/abs/1510.07640).
- [5] H. Ishikawa, M. Yoshida, K. Nawa, M. Jeong, S. Krämer, M. Horvatic, C. Berthier, M. Takigawa, M. Akaki, A. Miyake, M. Tokunaga *et al.*, *Phys. Rev. Lett.* **114**, 227202 (2015).
- [6] O. Janson, S. Furukawa, T. Momoi, P. Sindzingre, J. Richter, and K. Held, [arXiv:1509.07333](https://arxiv.org/abs/1509.07333).
- [7] A. V. Chubukov, *Phys. Rev. B* **44**, 4693 (1991).
- [8] L. Kecke, T. Momoi, and A. Furusaki, *Phys. Rev. B* **76**, 060407 (2007).
- [9] T. Vekua, A. Honecker, H.-J. Mikeska, and F. Heidrich-Meisner, *Phys. Rev. B* **76**, 174420 (2007).
- [10] T. Hikihara, L. Kecke, T. Momoi, and A. Furusaki, *Phys. Rev. B* **78**, 144404 (2008).
- [11] J. Sudan, A. Lüscher, and A. M. Läuchli, *Phys. Rev. B* **80**, 140402 (2009).
- [12] D. V. Dmitriev and V. Y. Krivnov, *Phys. Rev. B* **79**, 054421 (2009).
- [13] M. Zhitomirsky and H. Tsunetsugu, *Europhys. Lett.* **92**, 37001 (2010).
- [14] L. Svistov, T. Fujita, H. Yamaguchi, S. Kimura, K. Omura, A. Prokofiev, A. I. Smirnov, Z. Honda, and M. Hagiwara, *Pis'ma v ZhETF* **93**, 24 (2011) [*JETP Lett.* **93**, 21 (2011)].
- [15] A. V. Syromyatnikov, *Phys. Rev. B* **86**, 014423 (2012).
- [16] A. V. Sizanov and A. V. Syromyatnikov, *Phys. Rev. B* **87**, 014410 (2013).
- [17] M. Enderle, C. Mukherjee, B. Fåk, R. K. Kremer, J.-M. Broto, H. Rosner, S.-L. Drechsler, J. Richter, J. Málek, A. Prokofiev *et al.*, *Europhys. Lett.* **70**, 237 (2005).
- [18] N. Büttgen, H.-A. Krug von Nidda, L. E. Svistov, L. A. Prozorova, A. Prokofiev, and W. Aßmus, *Phys. Rev. B* **76**, 014440 (2007).
- [19] N. Büttgen, W. Kraetschmer, L. E. Svistov, L. A. Prozorova, and A. Prokofiev, *Phys. Rev. B* **81**, 052403 (2010).
- [20] M. Hagiwara, L. Svistov, T. Fujita, H. Yamaguchi, S. Kimura, K. Omura, A. Prokofiev, A. I. Smirnov, and Z. Honda, *J. Phys.: Conf. Ser.* **320**, 012049 (2011).
- [21] M. Sato, T. Hikihara, and T. Momoi, *Phys. Rev. Lett.* **110**, 077206 (2013).
- [22] S.-L. Drechsler, O. Volkova, A. N. Vasiliev, N. Tristan, J. Richter, M. Schmitt, H. Rosner, J. Málek, R. Klingeler, A. A. Zvyagin *et al.*, *Phys. Rev. Lett.* **98**, 077202 (2007).
- [23] M. Schmitt, J. Málek, S.-L. Drechsler, and H. Rosner, *Phys. Rev. B* **80**, 205111 (2009).
- [24] M. Matsuda, H. Yamaguchi, T. Ito, C. H. Lee, K. Oka, Y. Mizuno, T. Tohyama, S. Maekawa, and K. Kakurai, *Phys. Rev. B* **63**, 180403 (2001).
- [25] R. Kuzian, S. Nishimoto, S.-L. Drechsler, J. Málek, S. Johnston, J. van den Brink, M. Schmitt, H. Rosner, M. Matsuda, K. Oka *et al.*, *Phys. Rev. Lett.* **109**, 117207 (2012).
- [26] A. Wolter, F. Lipps, M. Schäpers, S.-L. Drechsler, S. Nishimoto, R. Vogel, V. Kataev, B. Büchner, H. Rosner, M. Schmitt *et al.*, *Phys. Rev. B* **85**, 014407 (2012).
- [27] B. Willenberg, M. Schäpers, K. C. Rule, S. Süllow, M. Reehuis, H. Ryll, B. Klemke, K. Kiefer, W. Schottenhamel, B. Büchner *et al.*, *Phys. Rev. Lett.* **108**, 117202 (2012).
- [28] M. Schäpers, A. Wolter, S. Drechsler, S. Nishimoto, K.-H. Müller, M. Abdel-Hafiez, W. Schottenhamel, B. Büchner, J. Richter, B. Ouladdiaf *et al.*, *Phys. Rev. B* **88**, 184410 (2013).
- [29] M. Hase, H. Kuroe, K. Ozawa, O. Suzuki, H. Kitazawa, G. Kido, and T. Sekine, *Phys. Rev. B* **70**, 104426 (2004).
- [30] W. E. A. Lorenz, R. Kuzian, S.-L. Drechsler, W.-D. Stein, N. N. Wizen, G. Behr, J. Málek, U. Nitzsche, H. Rosner, A. Hiess *et al.*, *Europhys. Lett.* **88**, 37002 (2009).
- [31] S. Nishimoto, S.-L. Drechsler, R. O. Kuzian, J. van den Brink, J. Richter, W. E. A. Lorenz, Y. Skourski, R. Klingeler, and B. Büchner, *Phys. Rev. Lett.* **107**, 097201 (2011).
- [32] R. O. Kuzian and S.-L. Drechsler, *Phys. Rev. B* **75**, 024401 (2007).
- [33] S. Nishimoto, S.-L. Drechsler, R. Kuzian, J. Richter, J. Málek, M. Schmitt, J. van den Brink, and H. Rosner, *Europhys. Lett.* **98**, 37007 (2012).
- [34] S. Nishimoto, S.-L. Drechsler, R. Kuzian, J. J. Richter, and J. van den Brink, *J. Phys.: Conf. Ser.* **400**, 032069 (2012).
- [35] S. Tornow, O. Entin-Wohlman, and A. Aharony, *Phys. Rev. B* **60**, 10206 (1999).
- [36] V. Yushankhai and R. Hayn, *Europhys. Lett.* **47**, 116 (1999).
- [37] V. Kataev, K.-Y. Choi, M. Grüninger, U. Ammerahl, B. Büchner, A. Freimuth, and A. Revcolevschi, *Phys. Rev. Lett.* **86**, 2882 (2001).
- [38] F. Heidrich-Meisner, I. P. McCulloch, and A. K. Kolezhuk, *Phys. Rev. B* **80**, 144417 (2009).
- [39] B. Willenberg, M. Schäpers, A. U. B. Wolter, S.-L. Drechsler, M. Reehuis, B. Büchner, A. J. Studer, K. C. Rule, B. Ouladdiaf, S. Süllow, and S. Nishimoto, [arXiv:1508.02207](https://arxiv.org/abs/1508.02207) [Phys. Rev. Lett. (to be published)].
- [40] O. Starykh and L. Balents, *Rep. Prog. Phys.* **75**, 052502 (2015).
- [41] O. A. Starykh and L. Balents, *Phys. Rev. B* **89**, 104407 (2014).

- [42] M. Mourigal, M. Enderle, M. Fak, R. K. Kremer, J. M. Law, A. Schneidewind, A. Hiess, and A. Prokofiev, *Phys. Rev. Lett.* **109**, 027203 (2012).
- [43] H. T. Ueda and K. Totsuka, [arXiv:1406.1960](https://arxiv.org/abs/1406.1960).
- [44] S. White, *Phys. Rev. Lett.* **69**, 2863 (1992).
- [45] S. Nishimoto, M. Nakamura, A. O'Brien, and P. Fulde, *Phys. Rev. Lett.* **104**, 196401 (2010).
- [46] E. Stoudenmire and S. R. White, *Annu. Rev. Condens. Matter Phys.* **3**, 111 (2012).
- [47] R. Zinke, S.-L. Drechsler, and J. Richter, *Phys. Rev. B* **79**, 094425 (2009).
- [48] Here and below, we use the presentation in terms of interpenetrating single Heisenberg chains coupled by J_1 , which includes explicitly both the limit of two decoupled Heisenberg chains $1/\alpha = 0$, and the quantum critical point $1/\alpha = 4$.
- [49] In order to see the equivalence of Eq. (7) with Eq. (37) of Ref. [32], we should substitute $J_1^{xy} = -1$, $J_1^z = -\Delta_1$, $J_2^{xy} = \alpha$, $J_2^z = \alpha\Delta_2$, $\mu B = h$ into the first line of Eq. (37). Unfortunately, the second line of this equation contains a misprint in the last term of its numerator. The correct expression reads as
- $$B_s = \frac{J_2^{xy}}{2\mu} \left[\frac{2(\Delta_2 + 1) - (\Delta_1/\alpha_7)^2 - 2\Delta_1\Delta_2/\alpha_7}{1 - \Delta_1/\alpha_7} \right].$$
- Note also that in the Ref. [32] the frustration ratio was defined as $\alpha_7 = J_2^{xy}/J_1^{xy} = -\alpha$.
- [50] H. T. Ueda and K. Totsuka, *Phys. Rev. B* **80**, 014417 (2009).
- [51] S.-L. Drechsler, S. Nishimoto, R. O. Kuzian, J. Málek, W. E. A. Lorenz, J. Richter, J. van den Brink, M. Schmitt, and H. Rosner, *Phys. Rev. Lett.* **106**, 219701 (2011).
- [52] A. A. Gippius, E. N. Morozova, A. S. Moskvin, A. V. Zalesky, A. A. Bush, M. Baenitz, H. Rosner, and S.-L. Drechsler, *Phys. Rev. B* **70**, 020406 (2004).
- [53] T. Masuda, A. Zheludev, B. Roessli, A. Bush, M. Markina, and A. Vasiliev, *Phys. Rev. B* **72**, 014405 (2005).
- [54] S. Drechsler, J. Richter, A. A. Gippius, A. Vasiliev, A. A. Bush, A. S. Moskvin, J. Málek, Y. Prots, W. Schnelle, and H. Rosner, *Europhys. Lett.* **73**, 83 (2006).
- [55] L. Mihály, B. Dóra, A. Ványolos, H. Berger, and L. Forró, *Phys. Rev. Lett.* **97**, 067206 (2006).
- [56] M. Enderle, B. Fåk, H.-J. Mikeska, R. K. Kremer, A. Prokofiev, and W. Assmus, *Phys. Rev. Lett.* **104**, 237207 (2010).
- [57] S. Yasui, Y. Yanagisawa, M. Sato, and I. Terasaki, *J. Phys.: Conf. Ser.* **320**, 012087 (2011).
- [58] This figure has been employed already in the preprint version of the present work ([arXiv:1303.1933](https://arxiv.org/abs/1303.1933)) and later on also in our recent paper devoted to linarite [28].
- [59] N. Büttgen, K. Nawu, T. Fujita, M. Hagiwara, P. Kuhns, A. Prokofiev, A. P. Reyes, L. E. Svistov, K. Yoshimura, and M. Takigawa, *Phys. Rev. B* **90**, 134401 (2014).
- [60] L. Prozorova, S. Sosin, L. Svistov, N. Büttgen, J. Kemper, A. Reyes, S. Riggs, O. Petrenko, and A. Prokofiev, [arXiv:1501.03226](https://arxiv.org/abs/1501.03226).
- [61] H. T. Ueda, *J. Phys. Soc. Jpn.* **84**, 023601 (2015).
- [62] E. Economou, *Green's Functions in Quantum Physics* (Springer-Verlag, Berlin, 2006).